AD NUMBER

ADB222178

NEW LIMITATION CHANGE

TO

Approved for public release, distribution unlimited

FROM

Distribution authorized to DoD only; Proprietary Info.; Oct 96. Other requests shall be referred to Phillips Lab., Kirtland AFB, NM 87117-5776.

AUTHORITY

Phillips Lab [AFMC], Kirtland AFB, NM ltr dtd 28 Jul 97

PL-TR-
97-1014

ROTARY CRYOGENIC THERMAL COUPLING

Dr. Alfred L. Johnson

Electro Thermo Associates
504 The Strand
Manhattan Beach, CA 90266

October 1996

Final Report

PHILLIPS LABORATORY
Space Technology Directorate
AIR FORCE MATERIEL COMMAND
KIRTLAND AIR FORCE BASE, NM 87117-5776

PL-TR-97-1014

Using Government drawings, specifications, or other data included in this document for any purpose other than Government procurement does not in any way obligate the U.S. Government. The fact that the Government formulated or supplied the drawings, specifications, or other data, does not license the holder or any other person or corporation; or convey any rights or permission to manufacture, use, or sell any patented invention that may relate to them.

This report contains proprietary information and shall not be either released outside the government, or used, duplicated or disclosed in whole or in part for manufacture or procurement, without the written permission of the contractor. This legend shall be marked on any reproduction hereof in whole or in part.

If you change your address, wish to be removed from this mailing list, or your organization no longer employs the addressee, please notify PL/VTV, 3550 Aberdeen Ave SE, Kirtland AFB, NM 87117-5776.

Do not return copies of this report unless contractual obligations or notice on a specific document requires its return.

This report has been approved for publication.

Marko Stoyanof
Marko Stoyanof
Project Manager

FOR THE COMMANDER

L. Kevin Slimak

L. KEVIN SLIMAK, GM-15
Chief, Space Vehicle Technologies Division

CHRISTINE M. ANDERSON, SES
Director, Space Technology Directorate

DRAFT SF 298

1. Report Date (dd-mm-yy) October 1996	2. Report Type Final	3. Dates covered (from... to) 11/95 - 10/96
4. Title & subtitle Rotary Cryogenic Thermal Coupling		5a. Contract or Grant # F29601-95-C-0133
		5b. Program Element # 62173C
6. Author(s) Dr. Alfred L. Johnson		5c. Project # 1602
		5d. Task # C0
		5e. Work Unit # ET
7. Performing Organization Name & Address Electro Thermo Associates 504 The Strand Manhattan Beach, CA 90266		8. Performing Organization Report # ETA SBIR\95\RTC006
9. Sponsoring/Monitoring Agency Name & Address Phillips Laboratory 3550 Aberdeen Ave. SE Kirtland, AFB 87117-5776		10. Monitor Acronym
		11. Monitor Report # PL-TR-97-1014

12. Distribution/Availability Statement
Distribution authorized to DoD components only; Proprietary Information; October 1996. Other requests for this document shall be referred to AFMC/STI.

13. Supplementary Notes

14. Abstract This Phase I Effort developed and demonstrated the principles and practices required for the design and fabrication of Rotary Cryogenic Thermal Couplers. A detailed mathematical thermal analysis of the radiant heat transfer occurring within the basic Rotary Cryogenic Thermal Coupling module was prepared. Module disk fin effectiveness versus the disk radius ratio and component dimensionless characterization parameter, I, was mapped for a specific temperature regime. The thermal analysis demonstrated that the thermal heat leak parasitic losses can be kept within a reasonable percentage of the transferred heat with the use of active thermal shielding. Preliminary design analysis concluded that the unproven, critical component portion of the Rotary Cryogenic Thermal Coupling was the basic radiation coupled disk assembly. Several alternate materials and processes approaches were considered The conclusion was that a concept based on vacuum brazed aluminum fabrication was the best option. A proof of concept module was designed and fabricated, which demonstrated that the module components can be fabricated.

15. Subject Terms Rotary Cryogenic Thermal Couplers

Security Classification of			19. Limitation of Abstract	20. # of Pages	21. Responsible Person (Name and Telephone #)
16. Report Unclassified	17. Abstract Unclassified	18. This Page Unclassified	limited	72	Marko Stoyanof (505) 846-0775

Government Purpose License Rights
(SBIR Program)

Contract Number: F29601-95-C-0133
Contractor: Electro Thermo Associates

This report contains proprietary data which was generated under the terms of a Federal Small Business Innovation Research (SBIR) contract. All such data is proprietary to the contractor for a period of four years after the completion of the project (Public Law 102-564). This data shall not be released outside the Department of Defense (DoD), or used, duplicated, or disclosed in whole or in part for manufacture or procurement, without the express written permission of the Contractor.

Executive Summary

Background.

The application of cryogenic refrigerators and similar cryogenic heat sinks to the cooling of scanning detectors on three axis stabilized spacecraft can be most effectively implemented by mounting the cryogenic heat sink on the despun portion of the vehicle and cooling the scanning sensor via a rotary cryogenic thermal coupling.

Phase I Effort.

The principles and practices required for the design and fabrication of a Rotary Cryogenic Thermal Coupling were developed and demonstrated.

A detailed mathematical analysis of the radiant heat transfer occurring within the basic Rotary Cryogenic Thermal Coupling module was prepared, including a mapping of the module disk fin effectiveness versus the disk radius ratio and a component dimensionless characterization parameter, λ, for a specific temperature regime.

A computer program was written to parametrically size a Rotary Thermal Coupler based on the mathematical analysis. A printout of the results of several different cases was presented.

The thermal analysis demonstrated that the thermal heat leak parasitic losses can be kept within a reasonable percentage of the transferred heat by incorporating active thermal shielding. The technology is applicable down to 10 K.

The preliminary design analysis concluded that the unproven, critical component portion of the Rotary Cryogenic Thermal Coupling was the basic radiation coupled disk assembly. Several alternate materials and processes approaches were considered. It was concluded that a concept based on vacuum brazed aluminum fabrication was the best option. A proof of concept module was designed and fabricated. This task demonstrated that the module components can be fabricated.

Phase II.

A proposal for Phase II was not submitted because there was no formal request issued by the contracting agency.

Table of Contents

List of Figures

1.0 IDENTIFICATION AND SIGNIFICANCE OF THE PROBLEM

Conceptually, the application of cryogenic refrigerators and similar cryogenic heat sinks to the cooling of scanning detectors on three axis stabilized spacecraft can be most effectively implemented by mounting the cryogenic heat sink on the despun portion of the vehicle and cooling the scanning sensor via a rotary cryogenic thermal coupling. If the cryogenic heat sink is to be either a cryogenic radiator or an expendable cryogenic fluid, vehicle geometry constraints usually show that it is impractical to mount the heat sink device on the scanning sensor segment. If a cryocooler is to be used, installing the cryogenic refrigerator (and its heat rejection thermal radiator) on the despun segment of the vehicle, which could be accomplished if a rotary cryogenic thermal coupler were utilized, would result in a reduction in weight, power, and sensor vibration and an increase in reliability.

Unfortunately, rotary cryogenic thermal coupling technology has yet to be demonstrated. This Phase I SBIR research and development activity establishes a basis for the design of such devices.

1.1 BACKGROUND

Consideration of the general problem of totally integrated spacecraft borne cryogenic thermal management systems indicates that rotary thermal couplings are required for some system implementations. A specific example would be to provide for the transfer of heat from a rotating (scanning) focal plane to a cryogenic heat sink located on de-spun segment of the spacecraft. The basic requirements for an acceptable rotary thermal coupling would be:

1. low thermal impedance;
2. negligible internal heat generation;

3. relatively low parasitic heat leak;
4. long service life;
5. high reliability;
6. relatively low mass;
7. low mechanical noise;
8. robust design to withstand ground handling shock and launch vibration;
9. convenient mounting/interface attachment provisions.

A literature survey found only one rotary thermal coupling design report[1], the abstract of which states:

> "This report documents the work to design, fabricate and test a rotating thermal joint for surveillance satellite applications. The rotating thermal joint uses heat pipe technology to transfer heat into and out of the joint. Heat is transferred through a liquid NaK filled annulus between the rotating and stationary portions of the joint. The joint has been shown to transfer 1500 watts with a 15C temperature drop."

This rotary thermal joint design is not useful in the cryogenic temperature range due to the use of the liquid metal. There is also a question of service life and reliability due to the requirement for a rotating mechanical seal to retain the liquid metal.

The design, fabrication, testing, installation, and unsuccessful launch of a mission specific rotary thermal coupler has been reported[2], but documentation is unavailable.

1.2 BASIC CONCEPT

Consideration of the general requirements for a rotary thermal coupling listed above suggests that the only truly compatible design must be based on radiant heat transfer between the rotating and stationary members. Given this design constraint, it is

apparent that there are only two possible geometrical variations; concentric cylinders and parallel disks. Figure 1 depicts these variations.

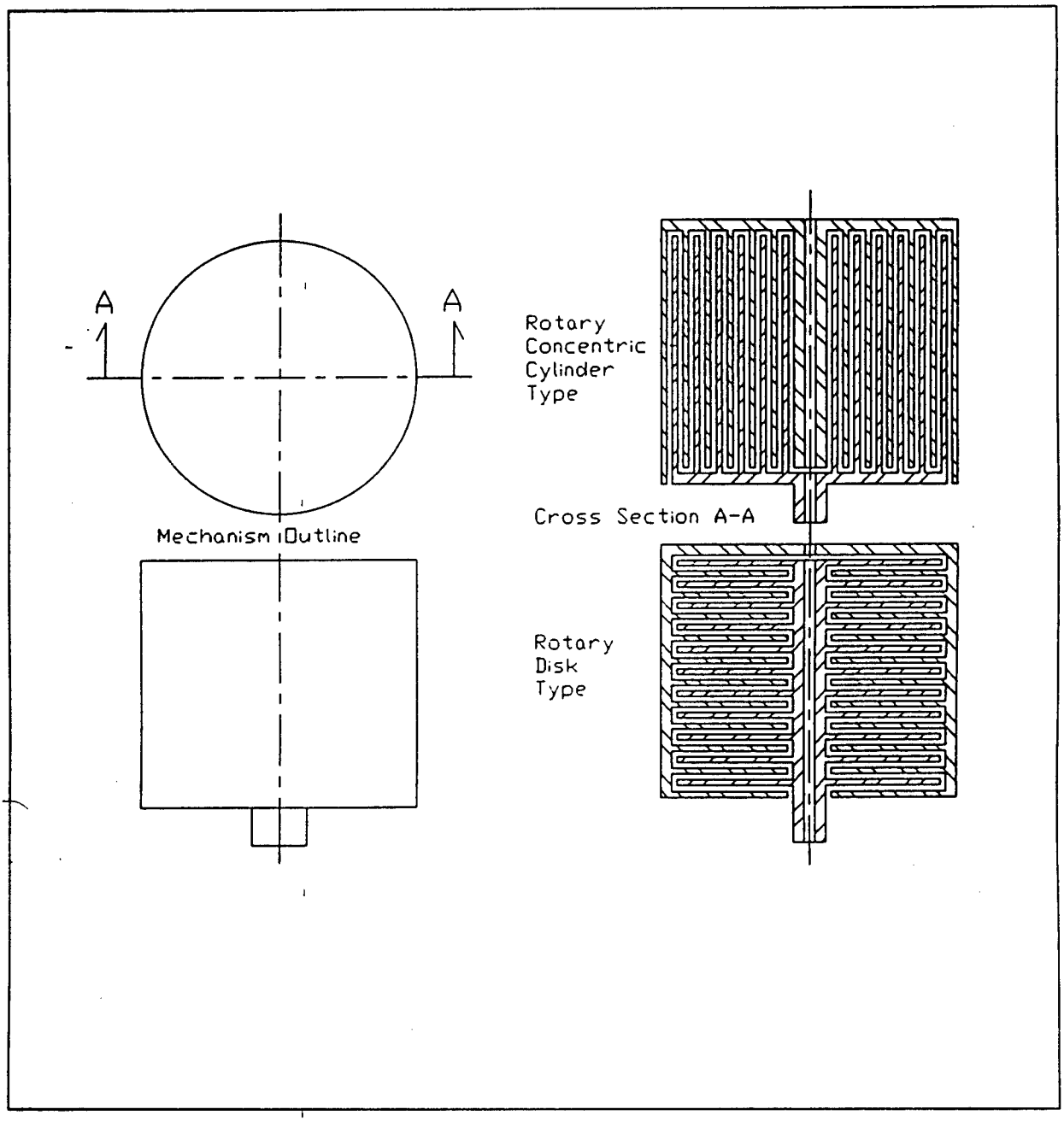

Figure 1 - Rotary Thermal Coupling Alternative Geometries

Figures 2 and 3 show isometric views detailing these alternate geometries

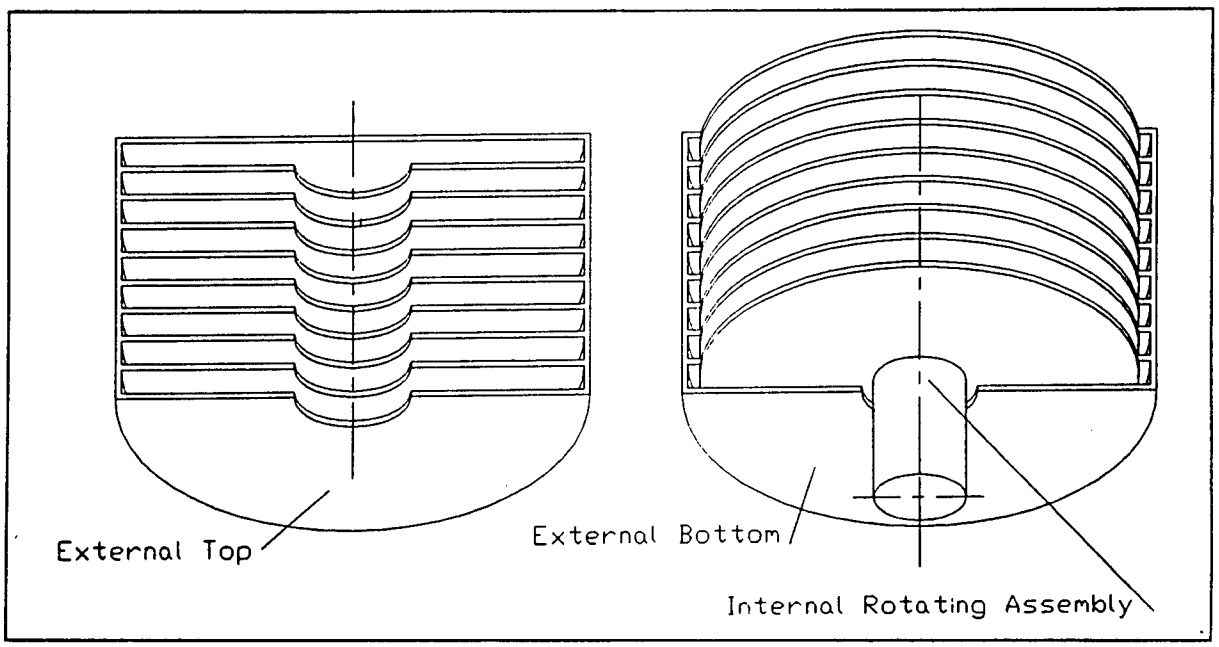

Figure 2 - Rotary Disk Thermal Coupling Isometric

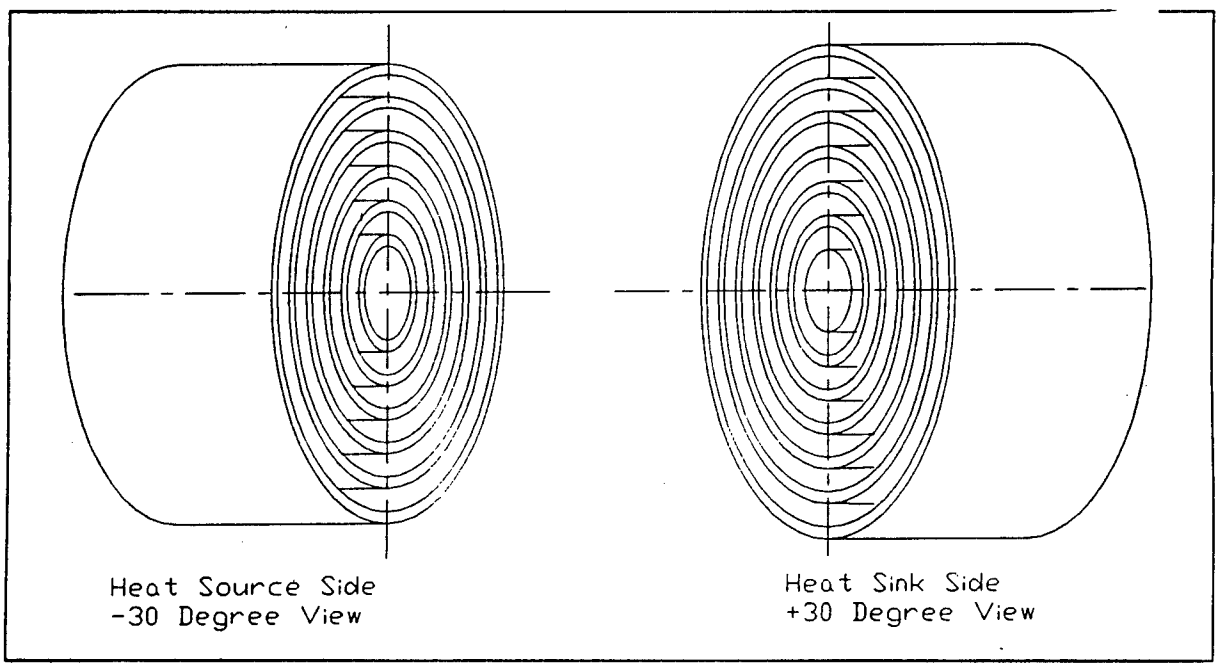

Figure 3 - Rotary Concentric Cylinder Thermal Coupling Isometric

To implement these coupling design concepts into a practical device, it is necessary to incorporate bearings, insulation, structural supports, housing, mounting, and interface provisions. For most installations the mounting interface will be a Bearing and Power Transfer Assembly (BAPTA). A BAPTA provides the basic structural, rotary support, rotary drive, power transfer, and control and data transfer between stationary and rotary segments of a space vehicle. BAPTA technology is well developed, with sources for providing "off-the-shelf" "state-of-the-art" hardware. The basic BAPTA configuration consists of the following elements:

outer stationary structural housing:
- provisions for mounting the stationary segment of the space vehicle,
- outer bearing race housings,
- drive motor stator mounting,
- power take-off stationary segment mounting,
- control and data assembly stationary segment mounting;

inner rotary structural housing:
- provisions for mounting the rotating segment of the space vehicle,
- inner bearing race housings,
- drive motor rotor mounting,
- power take-off rotary segment mounting,
- control and data assembly rotary segment mounting;

large diameter precision bearings;

large diameter, hollow shaft permanent magnet motor;

rotary transformer or slip ring power transfer subassembly;

control and data transfer assembly (optical or electromagnetic);

electrical connectors;

Figure 4 presents a general schematic of a BAPTA.

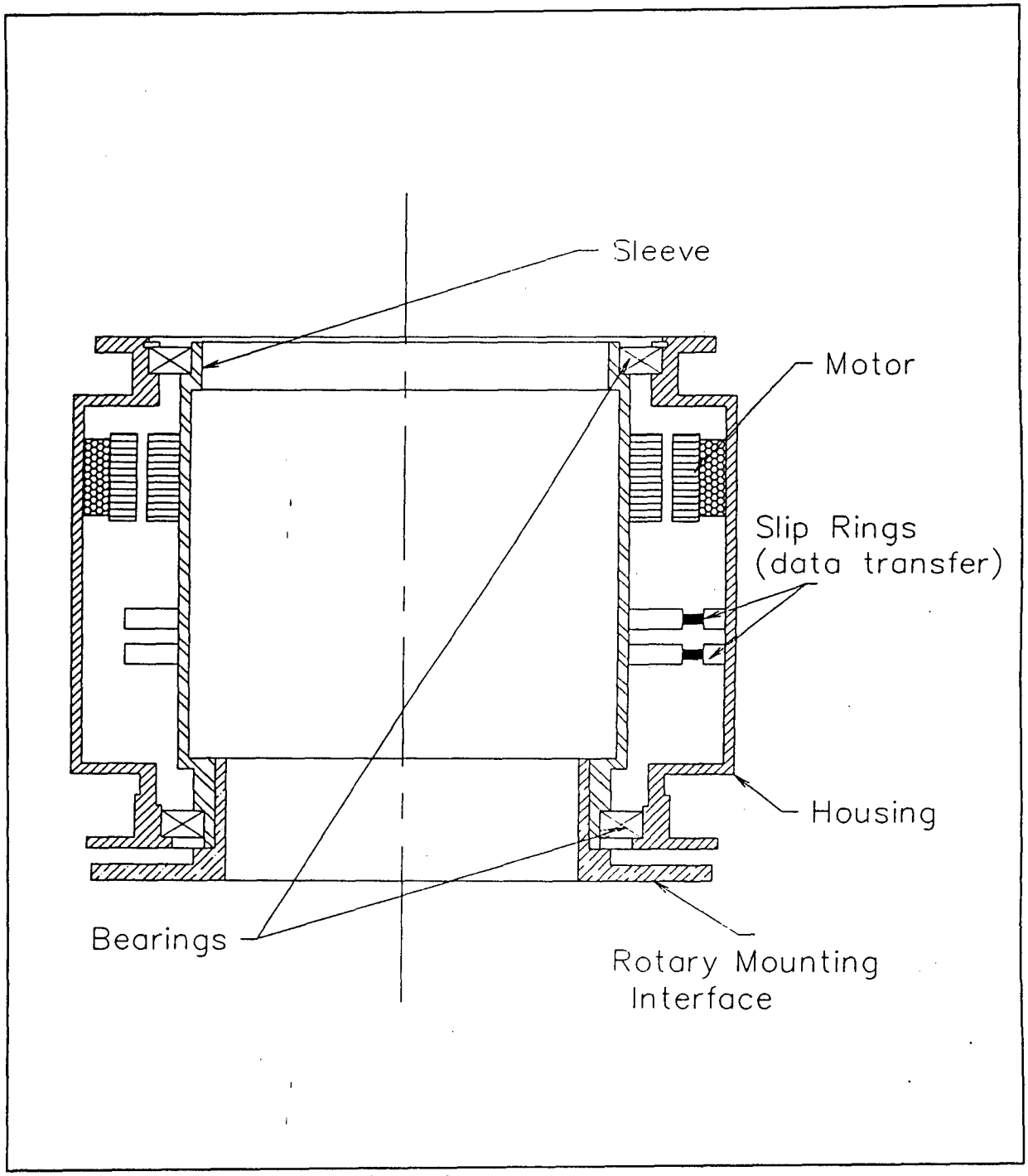

Figure 4 - BAPTA General Schematic

It is apparent that the BAPTA bearing support could be used also for the rotary thermal coupling bearing support in a highly integrated design. It is also apparent that provisions for compensating for alignment tolerances will be required for designs which incorporate the rotary thermal coupler as an appendaged subassembly to the BAPTA. The details of the bearing, support and thermal insulation design issues associated with a highly integrated BAPTA/Rotary Thermal Coupler are not addressed in this Phase I study nor are the alignment tolerance compensation issues associated with the appendaged subassembly approach. The Phase I study concentrates on the design issues associated with the basic rotary thermal coupler heat transfer module.

For the appendaged subassembly design approach, the issue of bearing integration with the basic rotary thermal coupler module warrants some preliminary consideration to establish the potential impact of these bearing systems on the basic rotary thermal coupler heat transfer module. There are two variations, a cold bearing design, and an ambient bearing design. Figures 5 and 6 show representative implementations using "cold" bearings while Figures 7 and 8 show representative implementations using ambient temperature bearings. It is evident from these figures that the rotary disk configuration has intrinsic design advantages over the rotary concentric cylinder configuration. The only case where the rotary concentric cylinder approach would be the configuration of choice would be if there were an advantage to a variable area coupling feature. By displacing the one set of cylinders axially from the second set, the coupling radiative area would change. It is possible to integrate a linear positioning device into the design so that the radiative coupling of the rotary concentric cylinder design could be controlled, thus providing a method of temperature control. This approach will not be explored as part of this research and development effort as it is beyond the scope of this SBIR program

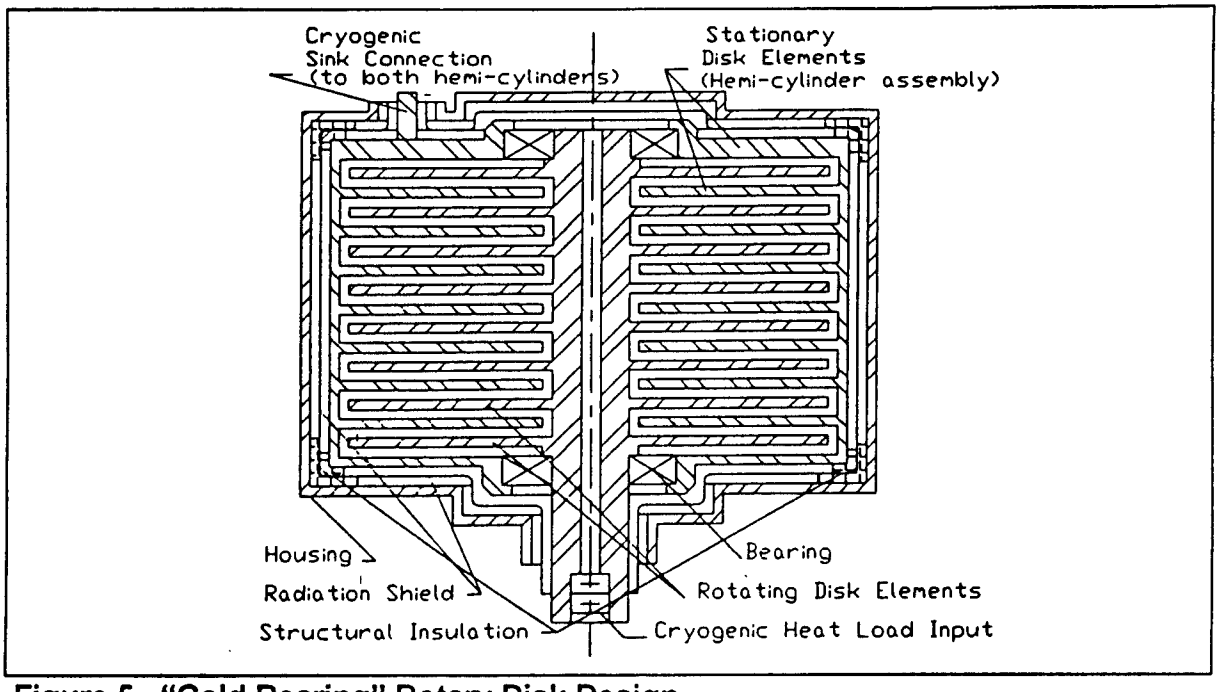

Figure 5 - "Cold Bearing" Rotary Disk Design

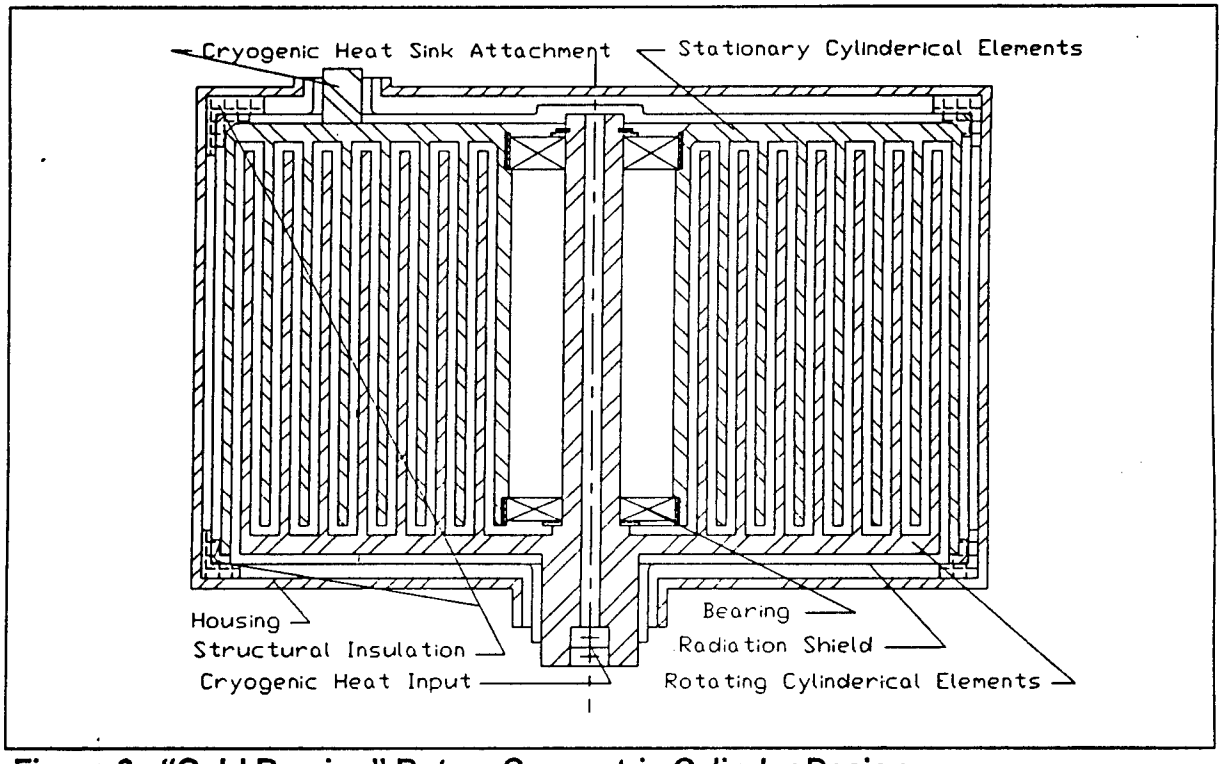

Figure 6 - "Cold Bearing" Rotary Concentric Cylinder Design

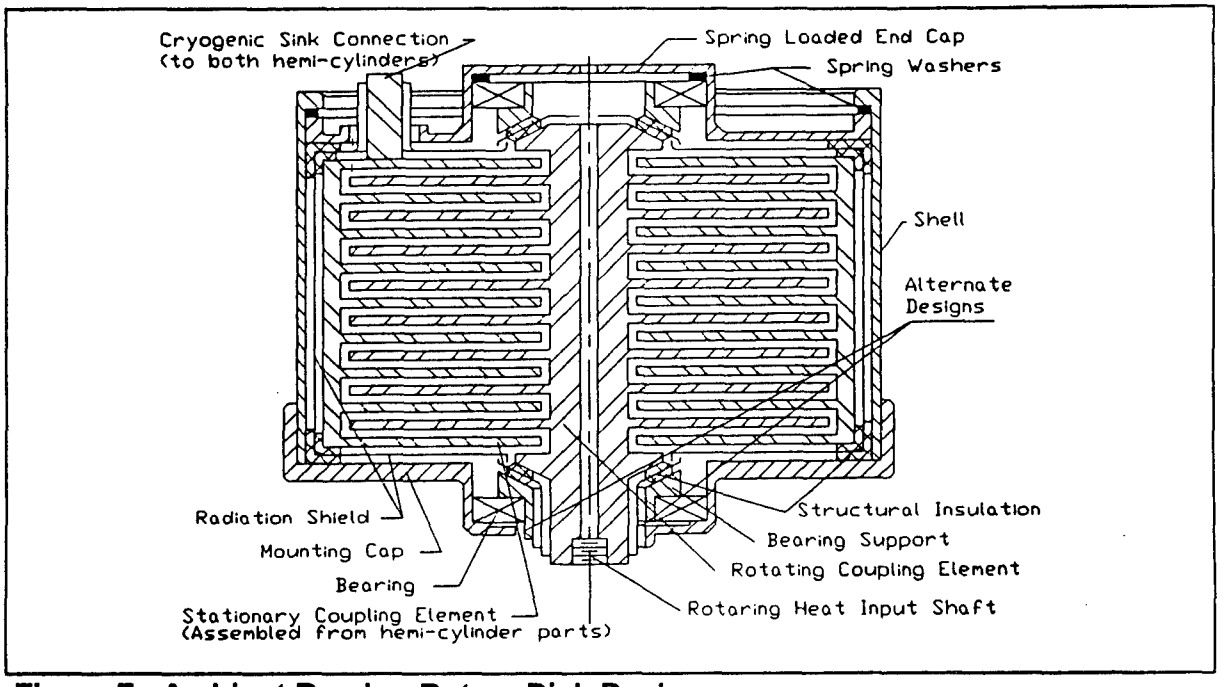

Figure 7 - Ambient Bearing Rotary Disk Design

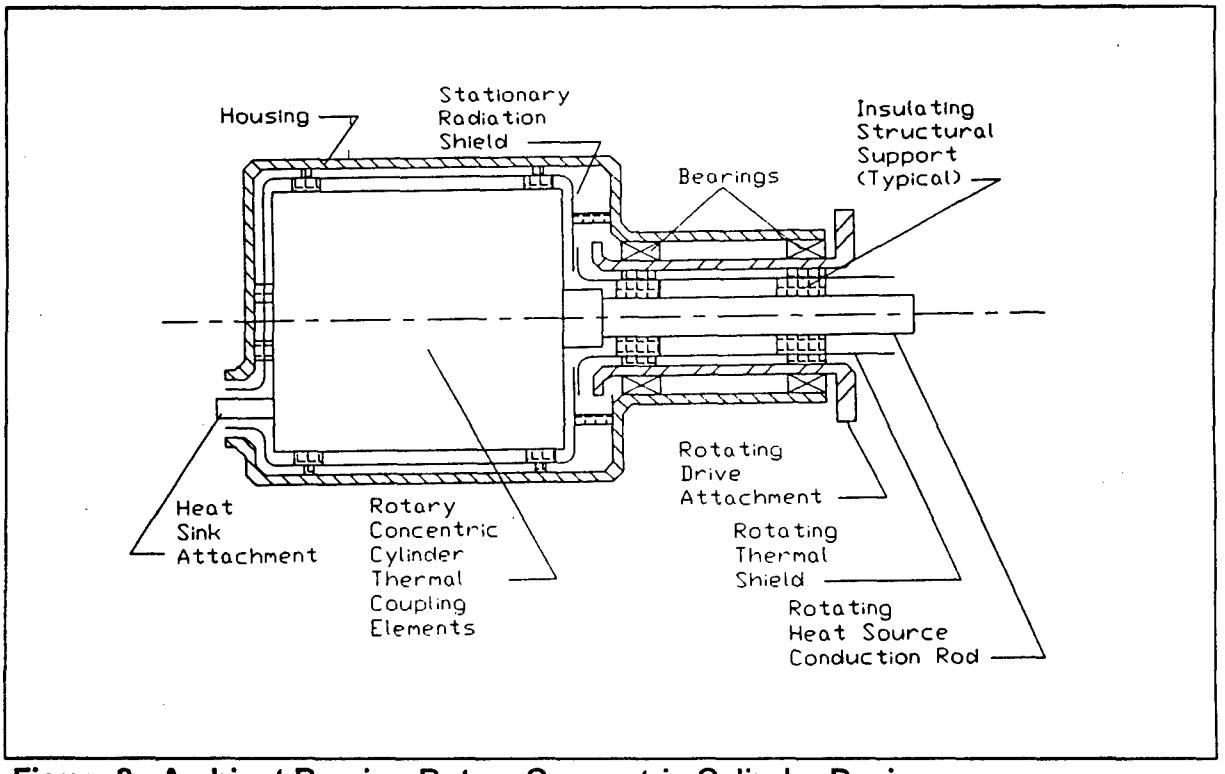

Figure 8 - Ambient Bearing Rotary Concentric Cylinder Design

The "cold" bearing design exhibits some mechanical assembly advantages over the ambient bearing design, however, the "cold" bearing will necessarily be of the dry lubricated type (lead, molybdenum disulfide, etc.)[3,4,5] while the ambient bearing design can be of the oil lubricated type (Barden precision bearing, ABEC 7, Bray oil lubricated, shielded metal retainer). The "cold" bearing has the further disadvantage that its frictional energy is dissipated within the cryogenic coupling path, thus adding a direct parasitic heat load. It does, however, introduce an additional conductive path. On the other hand, the ambient bearing design has intrinsically higher structural insulation parasitic effects. The ultimate choice between these two alternatives requires a detailed design analysis which will be undertaken under the Phase II activities.

Other design features shown in Figures 5 through 8 are the polished gold plated radiation shields, the provisions for interfacing with the rotating heat load and the stationary heat sink, the insulating structural mounting provisions, and the housing. To minimize the parasitic radiative heat load from the ambient housing to the coupling elements, the interior of the housing should be polished metal, preferably gold plated, as should be the external surface of the stationary element. To further reduce the radiative heat load, a single radiative shield is also included (at least in the initial design iteration). Consideration of the radiation equation applicable to such a system, which can be approximated adequately as per equation 1.0, it is evident that the addition of a single radiative shield will half the radiative heat leak.

$$\frac{Q_S}{A_S} = \frac{\sigma \varepsilon_S (T_S^4 - T_E^4)}{\left(1 + \left(\frac{A_S}{A_E}\right)\right)(n+1)} \qquad (1.0)$$

The rotating heat load interface is designed to be concentric with the axis of rotation. The stationary heat sink interface is located off axis. This configuration is convenient from a design viewpoint, and further, allows for the provision of a hole concentric with the axis of rotation that could be adapted to laser signal transmission from the rotating assembly to the fixed portion of the installation. Details for actual method of attachment to these thermal interfaces will be established during the Phase II research and development program. Consideration must be given to the effects of differential expansion of the axial dimensions of these interfaces during operation.

The insulating structural mounting provisions for the rotary cryogenic thermal coupler module must be carefully considered. The parasitic heat leak from the ambient housing to the cryogenic coupler elements needs to be kept to a small fraction of the heat transmitted from the rotating cold heat source. Techniques which can accomplish this include pyramid stacked ball compression supports, low conductance tension supports, and passive orbital disconnect devices,. Figure 9 shows the first technique.

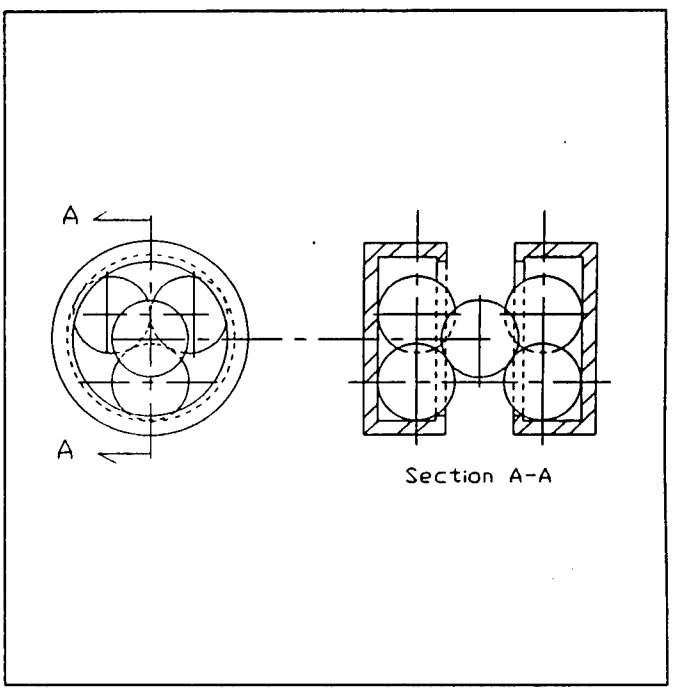

Figure 9 - Pyramid Stacked Ball Support

The insulating structural support must be capable of providing for the ground shock, handling, and the launch environment loads and vibration, must provide for the

differential thermal expansion between the housing mounting interface and the cryogenic coupling elements during operation, and must not introduce a large parasitic heat leak. Any of these techniques can be successfully adapted to the Rotary Cryogenic Thermal Coupler design, the appropriate selection being dependent upon the specific application. The pyramid stacked ball compression support is most useful in very low temperature, small size applications; the low conductance tension support is primarily intended for moderate size applications throughout the total temperature range; and the passive orbital disconnect devices being intended for heavy, large applications at the higher cryogenic temperature range. The design and integration of the detailed insulating structural supports will conducted as a major element of the Phase II segment of is program.

The housing provides the support points for the insulating cryogenic structural support, the mounting interface of the entire unit to the ambient vehicle structure, bearing support for the ambient temperature bearing design version, possibly provisions for compensating for the differential thermal expansion, and the envelope which ties all the parts together.

The rotary cryogenic thermal coupling elements can be fabricated of copper, aluminum, or a carbon fiber composite - high conduction material being mandatory for thermal efficiency and low weight. For the metallic designs, the elements can be fabricated from bar stock using plunge tool electrical discharge machining to cut the voids which surround the fins, or can be fabricated from copper pieces by diffusion bonding or from aluminum pieces by vacuum brazing. Soldering is not considered to be an acceptable process for this application due to excessive thermal impedance and the possibility of unacceptable thermally induced internal stresses.

The use of carbon fiber composites would require the application of adhesive bonding techniques. There are no apparent advantages to using this currently labor intensive, costly process.

To keep the size and weight low, the fins and the gaps should be kept as small as possible. The diffusion bonding and the vacuum brazing techniques require larger tolerances on the gaps to avoid contact due to the possible warping of the parts during the high temperature processes.

The fin thickness is constrained by both manufacturing limits and conduction fin effectiveness. It will be necessary to conduct a through thermal analysis of the integrated design to select the optimum fin thickness for any given design point. For very low temperature cryogenic couplers, the manufacturing limits and provisions for differential thermal expansion are anticipated to be the governing factors; for higher temperature applications, the fin effectiveness will most probably be the controlling feature.

Due to the simplicity of this design and the need for high design margins, it was initially proposed to use the linearized version of the radiation equation to account for the fin radiation boundary conditions. In this manner, the classical equations for fin effectiveness in a convective environment could be used rather than the more complex, radiation boundary conditions

The linearized form of the radiation equation is:

$$\frac{Q}{A} = \eta_f h_r (T_2 - T_1) \qquad (2.0)$$

The radiative heat transfer coefficient can be expressed as:

$$h_r=\sigma\varepsilon(T_2^3+T_2^2T_1+T_2T_1^2+T_1^3) \qquad (2..1)$$

The fin effectiveness is a function of h_r, the material thermal conductivity, the fin radius ratio, the fin thickness, and the radial dimension, which can be shown to be of the form:

$$\eta_f = f\left\langle (r_o - r_i)\sqrt{\frac{h_r}{k\delta}}\right\rangle \qquad (2.2)$$

From the literature survey, however, it was discovered that this linearization would result in optimistic performance predictions rather than conservative predictions. Chambers and Sommers[6] have shown that the use of the linear approximation overstated the fin effectiveness of circular fin radiating to a 0 K radiation environment by as much as 60%. Thus, an analysis of the rotary coupling module, including the effect of the 4^{th} power radiative heat transfer between the stationary and the rotating members was undertaken. A complete description of this analysis is presented in Section 3.

2.0 PHASE I OBJECTIVES

Table 1-1 through 1-3 summarize the Phase I effort on a task by task format.

PHASE I TASK REVIEW

Task	Description	Result	Comment
Program Plan Revision	Provides the opportunity to revise the program plan to include aspects of the technology which become evident between the proposal preparation and contract award.	Due to the technical capabilities and background knowledge of VTPT relating to the need and required characteristics for a Rotary Cryogenic Thermal Coupling, the Kick-Off and mid-term interface meetings were eliminated.	All interface communication was handled by telephone, FAX, and monthly progress reporting. This change increased the cost effectiveness of the program in that both parties would not have to prepare for non productive meetings.
Program Administration Programmatic Support	Covers the administrative functions which are unique to the contracted effort	Of all the activities included within this task, the coordination of the billing and reimbursement was more difficult than anticipated. A change in the contract administration from DCAMO - El Segundo to DCAMO - Van Nuys was not appropriately completed, resulting in the contract not being entered into the billing system.	The transmittal and processing of the DD 250 forms through the various approval offices resulted in a 6 month funding delay that caused an 8 month slippage in the completion of the Phase I effort.
Technical Direction	Responsible for all aspects of the technical direction of the program.	A review of the technical papers obtained in the literature survey necessitated the expansion of the scope of several tasks.	Principal Investigator must recognize when redirection is needed and know how to efficiently implement the required changes.
Conceptual Design	Prepare a conceptual design of the Rotary Cryogenic Thermal Coupling considering the integrated impact of critical component, materials, processes, and a preliminary thermal/structural analysis	Several alternative configurations were synthesized and evaluated. It was concluded that the rotary disk configuration is superior to the rotary concentric cylinder configuration	The method of integrating the coupler to the spacecraft BAPTA will significantly influence the design

Table 1 of 3

PHASE I TASK REVIEW

Task	Description	Result	Comment
Material Selection	Identify suitable materials Define methods for fabrication and bonding the rotary thermal coupling	The competitive materials are Aluminum and Copper. Titanium and Carbon Fiber composites were rejected as they did not offer any advantage.	The need for a high conductance thermal interface between the disks and spacers implied a need for metallurgical bonding. Forming a complete unit from solid bar stock was neither required nor cost effective
Processes and Manufacturing Controls	Select fabrication, handling, bonding, finishing, and assembly techniques.	Units to be fabricated from stock sheet stock, metallurgically bonded, wire EDM machines, high emmisivity surface finished, and assembled.	The Phase I effort limited the scope to the fabrication of the basic rotary cryogenic thermal coupling unit. Consideration was given to the mounting, thermal insulation, and interface requirements, however, no details were examined.
Preliminary Rotary Cryogenic Thermal Coupling design process	Prepare a preliminary design methodology for a Rotary Cryogenic Thermal Coupler	Based on a set of simplified characteristic bounding approximations, an initial preliminary design methodology was created.	The preliminary design methodology was to be improved by incorporating more exact thermal physical properties and modeling approximations during the Phase II effort

Table 2 of 3

PHASE I TASK REVIEW

Task	Description	Result	Comment
Fabricate a typical critical component	Fabricate a mechanical mockup to demonstrate the selected fabrication process	A preliminary design layout of a typical Rotary Cryogenic Thermal Coupler was prepared, sheet metal details for building a rotary thermal coupling module were prepared, the parts were assembled, vacuum brazed, and EDM machined.	The techniques demonstrated will be used to detail design and fabricate the "Pathfinder" engineering model early in the Phase II program.
Progress Reports	Prepare Monthly Progress Reports	5 Monthly Progress Reports were prepared and transmitted.	
Phase II Proposal	When and if requested, prepare a proposal for Phase II.	No request for a Phase II Proposal was received.	A Phase II task description was prepared in the course of conducting the Phase I effort. Comments are included throughout the Phase I Final Report indicating the scope of the Phase II effort
Final Report	Document the results of the Phase I program	These tables summarize the highlights of the Phase I program	The Phase I program successfully demonstrated the critical technologies needed for the Rotary Cryogenic Thermal Coupler

Table 3 of 3

3.0 ROTARY THERMAL COUPLER MODULE THERMAL ANALYSIS

The governing differential equations are developed from fundamental principles. Figure 10 is an isometric view of a set of rotary thermal coupler module elements.

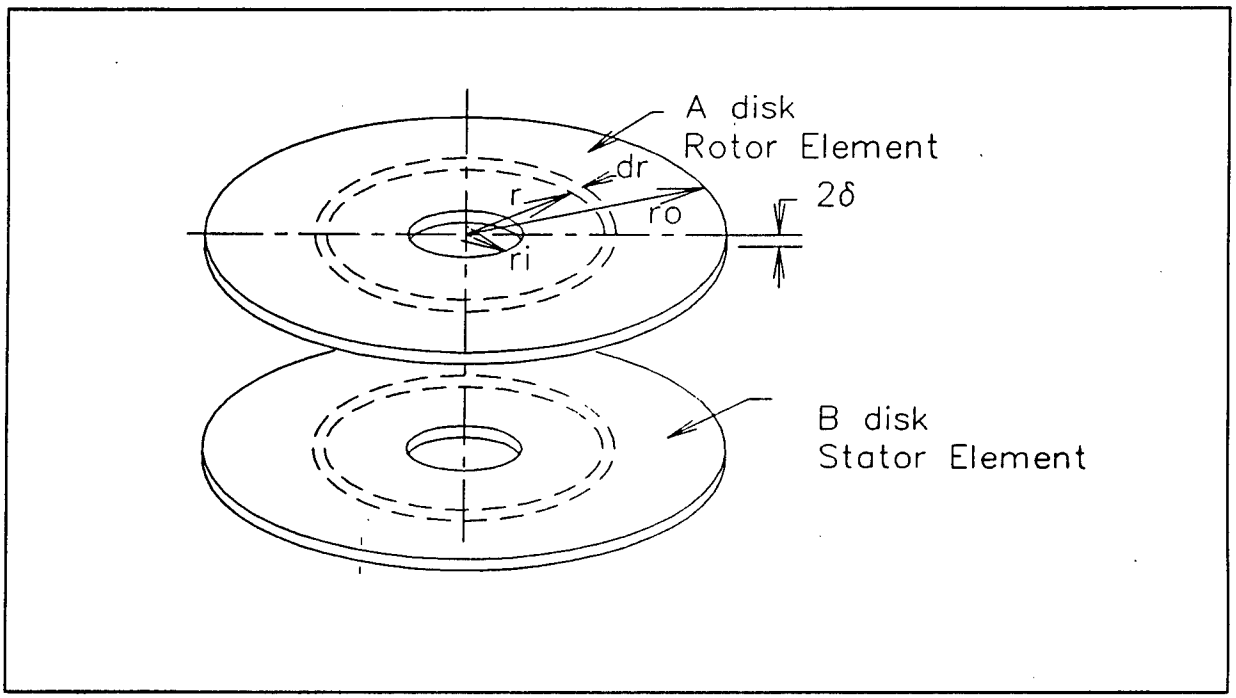

Figure 10 - Module Element Set Isometric

Figure 11 shows an idealized cross section through such a typical set of elements.

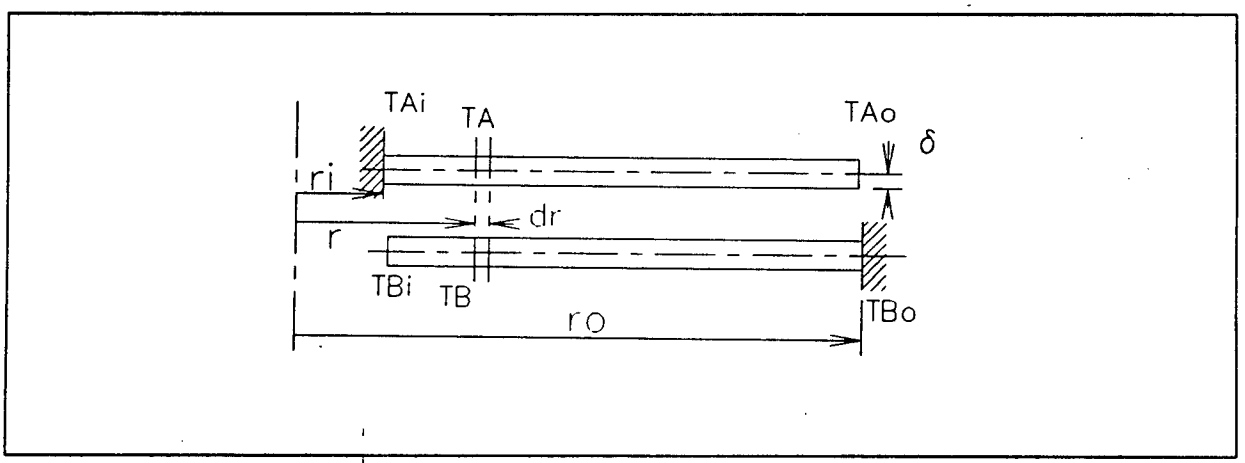

Figure 11- Module Element Set Thermal Characterization

The heat balance on the elemental differential volumes of the typical pair of disks can be graphically depicted as shown in Figure 12.

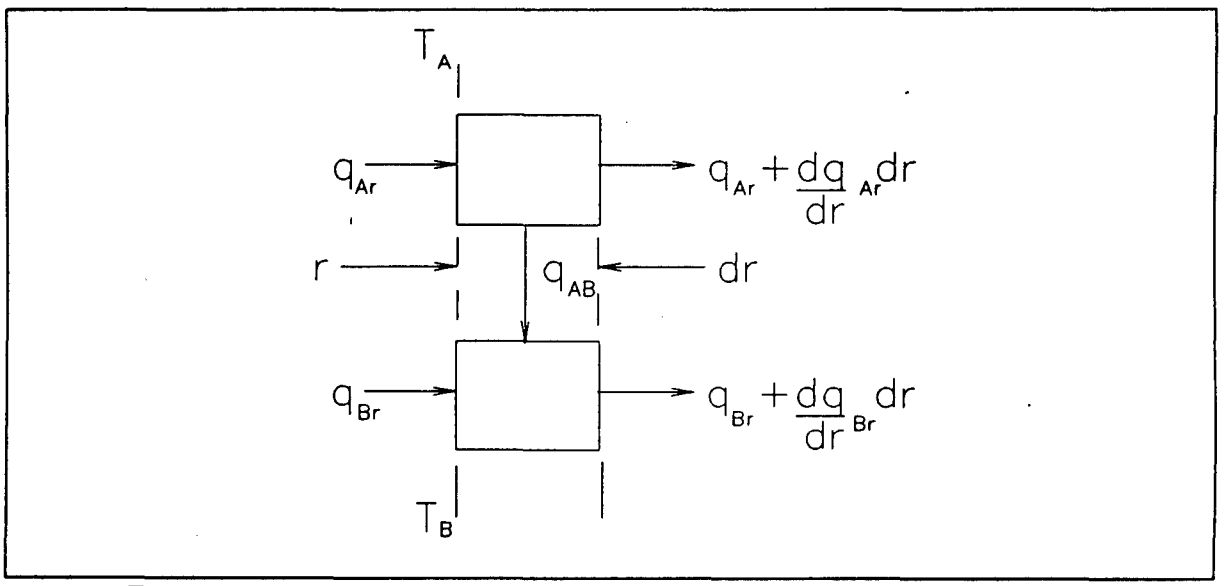

Figure 12 - Elemental Differential Volume Heat Balance Depiction

Based on the model shown above, the basic heat balance relationships are:

$$q_A = -2\pi r\delta k\frac{dT_A}{dr} \qquad (3.0)$$

$$q_B = -2\pi r\delta k\frac{dT_B}{dr} \qquad (3.1)$$

$$q_{AB} \leftrightharpoons -q_{BA} = \sigma\varepsilon F_{AB}2\pi r(T_A^4 - T_B^4)dr \qquad (3.2)$$

$$\frac{dq_A}{dr}dr = -2\pi\delta k\left(r\frac{d^2T_A}{dr^2} + \frac{dT_A}{dr}\right)dr = q_{BA} \qquad (3.3)$$

$$\frac{dq_B}{dr}dr = -2\pi\delta k\left(r\frac{d^2T_B}{dr^2} + \frac{dT_B}{dr}\right)dr = q_{AB} \qquad (3.4)$$

The analysis assumes that $T_A > T_B$, that the A disk is attached to the central rotating shaft, that the B disk is attached to the exterior cooled wall, and that the outer diameter of the A disk and the inner diameter of the B disk are effectively insulated. Note also

that δ is ½ the individual disk thickness, since the central plain through a disk is effectively adiabatic.

Consideration of the thermal boundary conditions imposed on a typical set of rotary thermal module elements implies that the temperature distribution through such a set will be as shown in Figure 13,

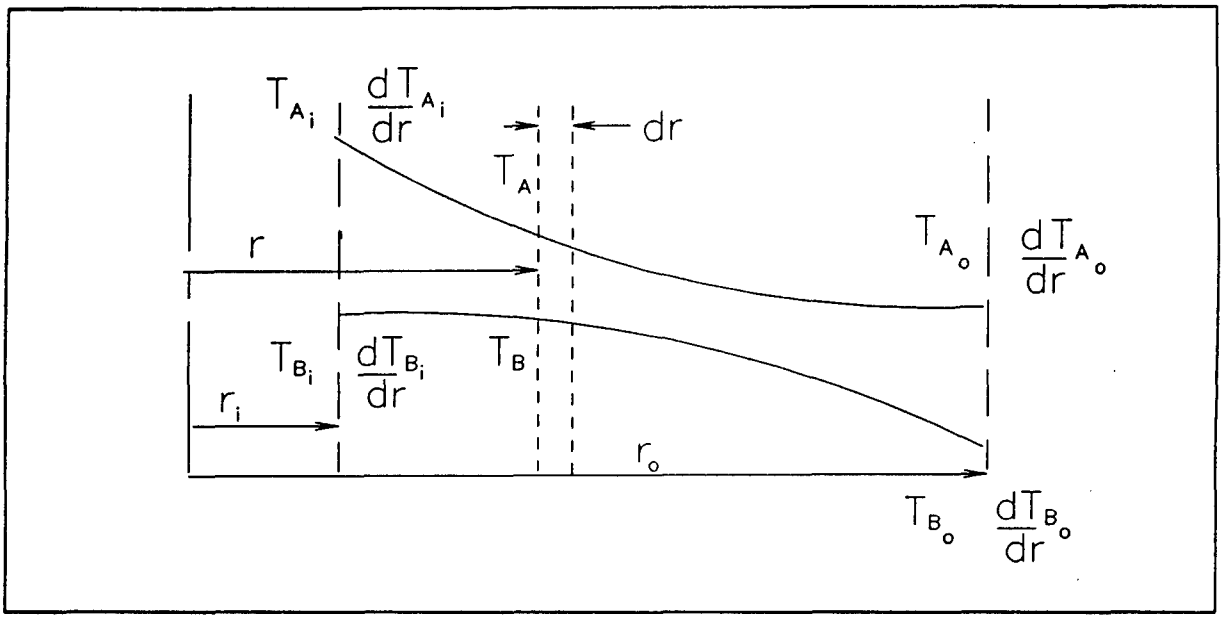

Figure 13 - Rotary Thermal Module Element Set Temperature Profile

From the foregoing, the differential equations governing the thermal steady state response of a pair of thermal elements can be expressed as:

$$\frac{d^2}{d}\frac{T_A}{r^2} + \frac{1}{r}\frac{dT_A}{dr} - \frac{\sigma\varepsilon F_{AB}(T_A^4 - T_B^4)}{k\delta} = 0 \qquad (4.0)$$

$$\frac{d^2}{d}\frac{T_B}{r^2} + \frac{1}{r}\frac{dT_B}{dr} + \frac{\sigma\varepsilon F_{BA}(T_A^4 - T_B^4)}{k\delta} = 0 \qquad (4.1)$$

subject to the following boundary conditions:

$$T_A = T_{Ai} \ @ \ r = r_i$$

$$\frac{dT_B}{dr} = 0 \ @ \ r = r_i$$

$$\frac{dT_A}{dr} = 0 \ @ \ r = r_o$$

$$T_B = T_{Bo} \ @ \ r = r_o$$

Equations 4.0 and 4.1 can be transformed to a more convenient form by using the following substitutions:

$$\Theta_A = \frac{T_A}{T_{Ai}};$$

$$\Theta_B = \frac{T_B}{T_{Ai}};$$

$$R = \frac{r - r_i}{r_o - r_i}$$

$$\rho = \frac{r_0}{r_i}$$

The resulting normalized equations are:

$$\frac{d^2}{d}\frac{\Theta_A}{R^2} + \frac{1}{R + \frac{1}{(r-1)}}\frac{d\Theta_A}{dR} - \frac{\sigma\varepsilon F_{AB} T_{Ai}^3 (r_o - r_i)^2 (\Theta_A^4 - \Theta_B^4)}{kd} = 0 \qquad (5.0)$$

$$\frac{d^2}{d}\frac{\Theta_B}{R^2} + \frac{1}{R + \frac{1}{(\rho-1)}}\frac{d\Theta_B}{dR} + \frac{\sigma\varepsilon F_{BA} T_{Ai}^3 (r_o - r_i)^2 (\Theta_A^4 - \Theta_B^4)}{k\delta} = 0 \qquad (5.1)$$

Equations 5.0 and 5.1 can be further simplified by introducing the dimensionless parameter:

$$\lambda = \frac{\sigma\varepsilon F_{AB} T_{Ai}^3 (r_o - r_i)^2}{k\delta} \qquad (5.2)$$

The form of the reduced normalized equations are:

$$\frac{d^2}{d}\frac{\Theta_A}{R^2} + \frac{1}{R + \frac{1}{(\rho-1)}}\frac{d\Theta_A}{dR} - \lambda(\Theta_A^4 - \Theta_B^4) = 0 \qquad (6.0)$$

$$\frac{d^2}{d}\frac{\Theta_B}{R^2} + \frac{1}{R + \frac{1}{(\rho-1)}}\frac{d\Theta_B}{dR} + \lambda(\Theta_A^4 - \Theta_B^4) = 0 \qquad (6.1)$$

The transformed boundary conditions for equations 6.0 and 6,1 are:

$$\Theta_A = 1 \text{ @ } R = 0$$

$$\frac{d\Theta_B}{dR} = 0 \text{ @ } R = 0$$

$$\frac{d\Theta_A}{dR} = 0 \text{ @ } R = 1$$

$$\Theta_B = \frac{T_{Bo}}{T_{Ai}} \text{ @ } R = 1$$

To aid in solving the coupled 2nd order nonlinear differential equations, 6.0 and 6.1, the following transformations can be used:

$$\frac{d\Theta_A}{dR} = \Omega \qquad (7.0)$$

$$\frac{d\Theta_B}{dR} = \Psi \qquad (7.1)$$

This allows equations 6.0 and 6.1 to be expressed as

$$\frac{d}{dR}\frac{\Omega}{R+\frac{1}{(\rho-1)}} - \lambda(\Theta_A^4 - \Theta_B^4) = 0 \qquad (7.2)$$

$$\frac{d}{dR}\frac{\Psi}{R+\frac{1}{(\rho-1)}} + \lambda(\Theta_A^4 - \Theta_B^4) = 0 \qquad (7.3)$$

with the corresponding boundary conditions being:

$$\Theta_A = 1 \text{ @ } R = 0$$

$$\Psi = 0 \text{ @ } R = 0$$

$$\Theta_B = \frac{T_{Bo}}{T_{Ai}} \text{ @ } R = 1$$

$$\Omega = 0 \text{ @ } R = 1$$

This set of four coupled 1st order nonlinear differential equations, subject to the boundary conditions, can be solved using numerical methods.

Note that from equations 6.0 and 6.1 the following relationship can be derived:

$$\frac{d^2\Theta_A}{dR^2}+\frac{1}{R+\frac{1}{(\rho-1)}}\frac{d\Theta_A}{dR}+\frac{d^2\Theta_B}{dR^2}+\frac{1}{R+\frac{1}{(\rho-1)}}\frac{d\Theta_B}{dR}=0 \qquad (8.0)$$

From which:

$$\frac{d^2(\Theta_A+\Theta_B)}{dR^2}+\frac{1}{R+\frac{1}{(\rho-1)}}\frac{d(\Theta_A+\Theta_B)}{dR}=0 \qquad (8.1)$$

By defining $\zeta=\Theta_A+\Theta_B$ equation 8.1 simplifies to:

$$\frac{d^2\zeta}{dR^2}+\frac{1}{R+\frac{1}{(\rho-1)}}\frac{d\zeta}{dR}=0 \qquad (9.0)$$

Now introducing the variable $\Phi=\frac{d\zeta}{dR}$, equation 9.0 transforms to

$$\frac{d\Phi}{dR}+\frac{\Phi}{R+\frac{1}{(\rho-1)}}=0 \qquad (10.0)$$

which results in the relationship:

$$\frac{d\Phi}{\Phi}=-\frac{dR}{R+\frac{1}{(\rho-1)}} \qquad (10.1)$$

The solution to equation 10.1 is:

$$\Phi=\Phi_0\frac{1}{[R(\rho-1)+1]} \qquad (11.0)$$

which inverse transforms into:

$$\frac{d\zeta}{dR}=\left.\frac{d\zeta}{dR}\right|_0\frac{1}{[R(\rho-1)+1]} \qquad (11.1)$$

and thence into:

$$\frac{d\Theta_A}{dR}+\frac{d\Theta_B}{dR}=\left(\frac{d\Theta_A}{dR}+\frac{d\Theta_B}{dR}\right)_0\frac{1}{[R(\rho-1)+1]} \qquad (11.2)$$

The solution to equation 11.1 is:

$$\zeta-\zeta_0=\left.\frac{d\zeta}{dR}\right|_0\frac{\ln[R(\rho-1)+1]}{(\rho-1)} \qquad (12.0)$$

which inverse transforms into:

$$(\Theta_A+\Theta_B)=(\Theta_A+\Theta_B)_0+(\left.\frac{d\Theta_A}{dR}\right|_0+\left.\frac{d\Theta_B}{dR}\right|_0)\frac{\ln[R(\rho-1)+1]}{(\rho-1)} \qquad (12.1)$$

Evaluating equation 11.2 at R=1 and applying the appropriate boundary conditions:

$$\left.\frac{d\Theta_B}{dR}\right|_1=\frac{1}{\rho}\left.\frac{d\Theta_A}{dR}\right|_0 \qquad (13.0)$$

which is simply the conservation of energy boundary condition. Evaluating equation 12.1 at R=1 and applying the appropriate boundary conditions:

$$(\Theta_A+\Theta_B)_1=(1+\Theta_B)_0+\left.\frac{d\Theta_A}{dR}\right|_0\frac{\ln(\rho)}{(\rho-1)} \qquad (14.0)$$

which proves to useful in developing a numerical analysis convergence criteria.

3.1 - RUNGE-KUTTA NUMERICAL ANALYSIS

The solution to the set of 1st order nonlinear differential equations 7.0 - 7.3 can be obtained by creating a vector, V_R, evaluated at R:

$$V_R \Leftarrow \left|\begin{matrix}\Theta_A\\ \Theta_B\\ \Omega\\ \Psi\end{matrix}\right|_R \qquad (15)$$

then substituting R and V_R into the vector $\frac{dV}{dR}$, to obtain $\left.\frac{dV}{dR}\right|_R$:

$$\left.\frac{dV}{dR}\right|_R \Leftarrow \begin{vmatrix} \frac{d\Theta_A}{dR} \\ \frac{d\Theta_B}{dR} \\ \frac{d\Omega}{dR} \\ \frac{d\Psi}{dR} \end{vmatrix} \Leftarrow R, V_R \qquad (16)$$

having obtained $\left.\frac{dV}{dR}\right|_R$, $V_{R+\Delta R}$ is then computed using the 4th order Runge-Kutta method.

The process starts at R=0 and proceeds to R=1 in steps of ΔR. The process is mathematically outlined below:

$$K_1 \leftarrow \Delta R \times \left.\frac{dV}{dR}\right|_R \leftarrow \left|\frac{dV}{dR}\right|_{R,V_R}$$

$$V_{K_1} \leftarrow V_R + \frac{K_1}{2}$$

$$R \leftarrow R + \frac{\Delta R}{2}$$

$$K_2 \leftarrow \Delta R \times \left.\frac{dV}{dR}\right|_{K_1,R} \leftarrow \left|\frac{dV}{dR}\right|_{R,V_{K_1}}$$

$$V_{K_2} \leftarrow V_R + \frac{K_2}{2}$$

$$K_3 \leftarrow \Delta R \times \left.\frac{dV}{dR}\right|_{K_2,R} \leftarrow \left|\frac{dV}{dR}\right|_{R,V_{K_2}}$$

$$R \leftarrow R + \frac{\Delta R}{2}$$

$$V_{K_3} \leftarrow V_R + K_3$$

$$K_4 \leftarrow \Delta R \times \left.\frac{dV}{dR}\right|_{K_3,R} \leftarrow \left|\frac{dV}{dR}\right|_{R,V_{K_3}}$$

$$V_{R+\Delta R} \leftarrow V_R + \frac{(K_1 + (2xK_2) + (2xK_3) + K_4)}{6}$$

The computation runs in (n+1) steps from R=0 to R=1 by $\Delta R = \frac{1}{n}$. After each loop, the results at R=1 are compared with the boundary conditions, the error computed, new input variables at R=0 are then generated using an algorithm designed to force convergence and the process repeated until the error is reduced to an acceptable value.

Given the temperature distribution, and the exact boundary conditions, the fin effectiveness can be computed from:

$$\eta_f = \frac{-2k\delta \left.\frac{dT_A}{dr}\right|_{r=r_i}}{\sigma\varepsilon(r_o^2 - r_i^2)(T_{Ai}^4 - T_{Boi}^4)} \qquad (17)$$

which reduces to the form:

$$\eta_f = \frac{-2\Omega_{R=0}}{\lambda(\rho - 1)(1 - \Theta_{B_{R=1}}^4)} \qquad (18)$$

A listing of the APL computer program which was written to compute the results of the analysis described above is provided in Appendix I. Several cases have been computed, the results of which are presented in Appendix II. Using these results Figure 14 plots η_f versus λ for various values of ρ and a specific value of $\Theta_{B_{R=1}}$.

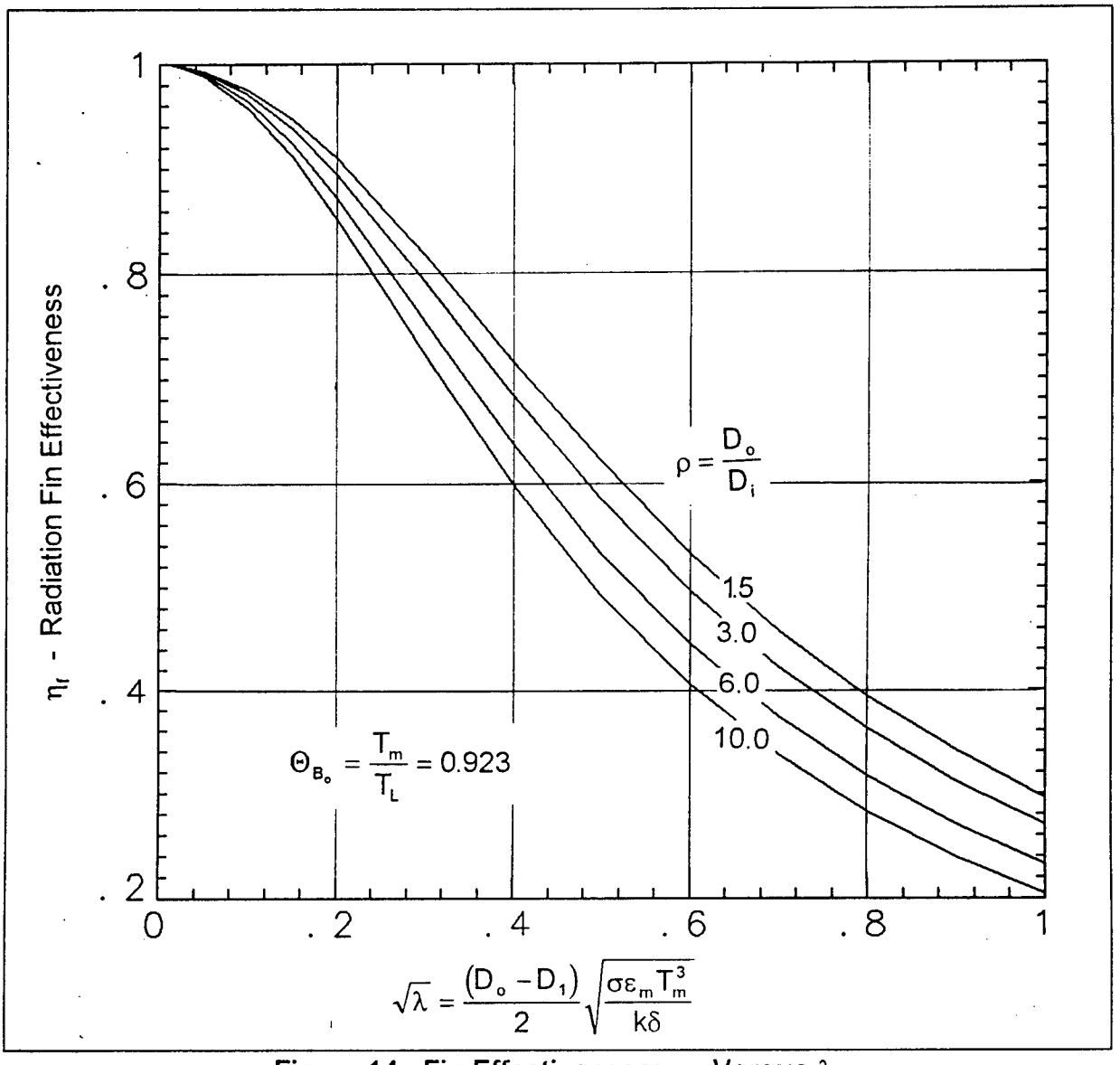

Figure 14 - Fin Effectiveness; η_f Versus λ, ρ

The computer program generates a complete Rotary Thermal Coupler design using the methodology described in the Section 4.0 Rotary Cryogenic Coupler Preliminary Design.

4.0 ROTARY CRYOGENIC THERMAL COUPLER PRELIMINARY DESIGN

The preliminary design is based on an the concept of an interleaved stack of radiantly thermally coupled disks, such as shown in Figure 2. Figure 15 defines the basic parameters which can be used to characterize such a module.

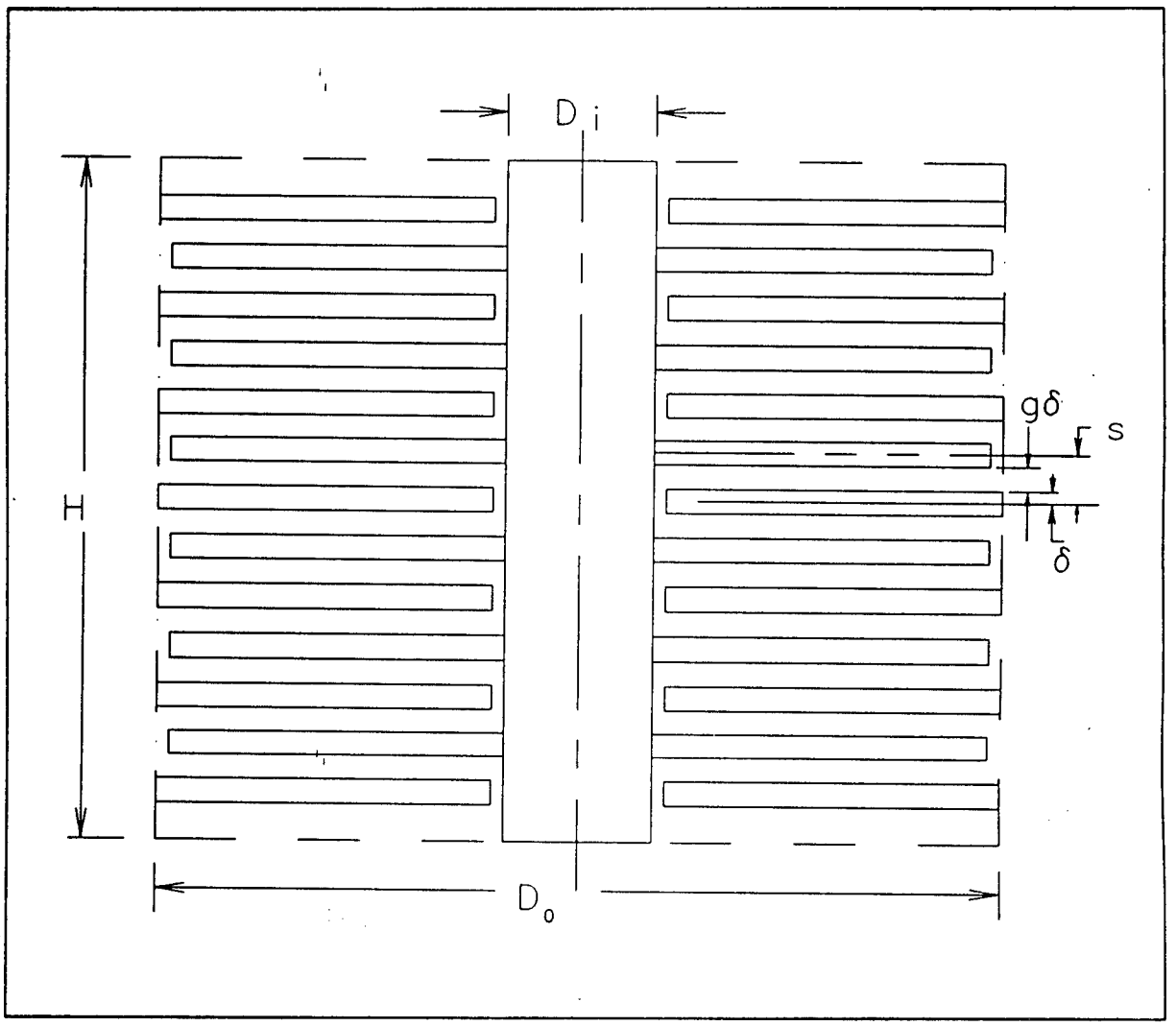

Figure 15 - Module Design Dimensional Parameters

Based on the parameters shown in Figure 15, the gap between an adjacent rotor-stator set of disks is $g\delta$. thus the distance between the adiabatic planes of an adjacent rotor-stator set of disks is:

$$s = (g+2)\delta$$

Given H, the overall height of stacked set of disks, the number of rotor-stator radiant interfaces, N, in a module is:

$$N = \frac{H}{s}$$

The nominal outside diameter of the thermally radiating area of a disk is denoted as D_o, the nominal inside diameter of the thermal radiating area of a disk is denoted as D_i. The effective coupled radiation area per module is thus:

$$\begin{aligned} A_m &= \frac{\pi\left(D_o^2 - D_i^2\right)}{4}N \\ &= \frac{\pi\left(D_o^2 - D_i^2\right)H}{4(g+2)\delta} \\ &= \frac{\pi\left(1 - \frac{D_i^2}{D_o^2}\right)D_o^2 H}{4(g+2)\delta} \end{aligned}$$

The overall diameter of a module is greater than D_o by twice the wall thickness of the stator, the wall thickness being established by the conditions imposed due to the combined influence of the need to provide a low thermal impedance conductive path coupling the module end plates with the stationary disk stack together with the annular area needed to provide sufficient surface area to assure that a sound, high conductance metallurgically bonded stack of disks can be fabricated.

The overall outside diameter of a complete Rotary Cryogenic Thermal Coupler will be greater than the overall outside diameter of a bonded module by twice the radial dimension required by the thermal support/insulation system. The height of a complete coupler will be the combined height of the module, the end plates, and the thermal support/insulation system. To minimize the parasitic heat leak into the module, it is desirable to maximize the internal volume per unit surface area. A cylinder with the height equal to the diameter has the maximum volume per unit surface area. Since the thickness of the thermal support/insulation system plus the conductive walls are approximately the same dimension axially as radially, the stack height of a module, H, excluding end plates, should be approximately equal to D_o, the outside diameter of the thermal radiating area of the module disks. Thus the net thermal radiation area per module is:

$$A_m = \frac{\pi\left(1-\left(\frac{1}{\rho}\right)^2\right)D_o^3}{4(g+2)\delta} \qquad (20.0)$$

Based on the fundamentals of radiation heat transfer and the relationships derived above, the governing equation for the heat transfer/module temperatures is:

$$Q_L = \eta_f A_m \sigma \varepsilon_m \left(T_L^4 - T_m^4\right) \qquad (21.0)$$

In conformance with the rotary thermal coupling module geometry, the insulating housing area can be defined as:

$$A_S = \pi D_S H_S + 2\frac{\pi D_S^2}{4} \qquad (22.0)$$

but $D_S = H_S$ in conformance with the shape of the rotary thermal coupling module.

Hence:

$$A_S = \frac{3\pi D_S^2}{2} \qquad (22.1)$$

Recalling equation 1.0, the governing equation for module housing heat leak is:

$$Q_S = \frac{\sigma \varepsilon_S A_S (T_S^4 - T_E^4)}{\left[1 + \left(\frac{A_S}{A_E}\right)\right](n+1)} \qquad (1.0)$$

By similar reasoning to that used in developing equation 22,1, it is apparent that:

$$A_E = \frac{3\pi D_E^2}{2} \qquad (23.0)$$

The identity $T_E = T_m$ is also evident, thus equation 1.0 can be revised to:

$$Q_S = \frac{\sigma \varepsilon_S A_S (T_S^4 - T_m^4)}{\left[1 + \left(\frac{D_S}{D_E}\right)^2\right](n+1)} \qquad (1.1)$$

By combining equations 1.1, 20.0, 21.0, 22.1, and 23.0, the ratio of the heat leak to the heat load can be expressed as:

$$\frac{Q_S}{Q_L} = \frac{6\varepsilon_S (g+2)\delta D_S^2 (T_S^4 - T_m^4)}{\eta_f \varepsilon_m \left(1 + \left(\frac{D_s}{D_E}\right)^2\right)(n+1)\left(1 - \left(\frac{1}{\rho}\right)^2\right) D_o^3 \left(T_m^4 - T_L^4\right)} \qquad (24.0)$$

By denoting $\Delta T_L = T_m - T_L$ where ΔT_L is the maximum temperature difference across the module, equation 24.0 can be expressed as:

$$\frac{Q_S}{Q_L} = \frac{6\varepsilon_S(g+2)\frac{\delta}{D_o}D_S^2\left(\left(\frac{T_S}{T_m}\right)^4 - 1\right)}{\eta_f\varepsilon_m\left(1+\left(\frac{D_s}{D_E}\right)^2\right)(n+1)\left(1-\left(\frac{1}{\rho}\right)^2\right)D_o^2\left(1-\left(1-\frac{\Delta T}{T_m}\right)^4\right)} \qquad (24.1)$$

Equation 24.1 is of interest because it is possible to introduce some order of magnitude approximations and obtain a quantitative expression for the relative heat leak. The order of magnitude approximations are:

$$\frac{D_S}{D_E} \approx 1.25$$

$$\frac{D_E}{D_o} \approx 1.10$$

$$\therefore \frac{D_S}{D_o} \approx 1.38$$

$$\rho \approx 4$$

$$\frac{\Delta T_L}{T_m} \approx 0.20$$

$$\frac{\delta}{D_o} \approx 0.0025$$

$$\frac{\varepsilon_S}{\varepsilon_m} \approx 0.03$$

$$(n+1) < 4$$

$$(g+2) > 3$$

$$\eta_f \approx 0.85$$

Thus the quantitative expression for the relative heat leak is:

$$\frac{Q_S}{Q_m} \geq 0.000618\left(\left(\frac{T_S}{T_m}\right)^4 - 1\right) \qquad (25.0)$$

For a typical application, T_S = 250 K, and T_m will be a value such as 10 K, 35 K, or 60 K, depending on the specific application. The corresponding relative heat leaks are then:

$$\left.\frac{Q_S}{Q_m}\right|_{10K}^{250K} = 241$$

$$\left.\frac{Q_S}{Q_m}\right|_{35K}^{250K} = 1.61$$

$$\left.\frac{Q_S}{Q_m}\right|_{60K}^{250K} = 0.19$$

It is apparent that the relative heat leak is not excessive for the 60 K application, and probably not excessive for the 35 K application, however, for the 10 K application, the relative heat leak would prove to be unacceptable.

To correct this situation, an active thermal shield could be incorporated within the insulation system. The active heat shield could be heat sunk to a 120 K thermal radiator. This would reduce the relative heat leak for these application to:

$$\left.\frac{Q_s}{Q_m}\right|_{10K}^{\frac{250K}{120K}} = 12.8$$

$$\left.\frac{Q_s}{Q_m}\right|_{35K}^{\frac{250K}{120K}} = 0.085$$

$$\left.\frac{Q_s}{Q_m}\right|_{60K}^{250K\,/\,120K} = 0.009$$

The reduction in relative heat leak for the 60 K application would not appear to be sufficient to justify the added complexity of an intermediate 120 K active heat shield , but it could be justified for the 35 K application. The relative heat leak for the 10 K application would probably still be unacceptable.

The difficulty with the 10 K application could be resolved by incorporating a 60 K active heat shield, the relative heat leak would reduce to:

$$\left.\frac{Q_s}{Q_m}\right|_{10K}^{60K} = 0.80$$

The 60 K heat sink could be provided by the first stage of the cryogenic refrigerator required to provide the 10 K heat sink that is to be transferred across the rotary cryogenic thermal coupling.

To reduce the heat load on the 1st stage of the cryogenic refrigerator, the addition of a 120 K active thermal shield within the rotary cryogenic thermal coupler insulation system should be considered.

The preceding analysis demonstrates the viability of the concept of the rotary cryogenic thermal coupler from a thermal management viewpoint. The importance of an adequate insulation system has been noted. Fortunately, the technology for providing such cryogenic insulation systems is state-of-the-art, including the incorporation of actively cooled shields integrated into the insulation system. To provide a more definitive mathematical description of a Rotary Thermal Coupler, the following analysis proves useful. First, rewrite equation 5.2 as:

$$\lambda = \frac{\sigma \varepsilon F_{AB} T_L^3 D_o^2 (1 - \frac{1}{\rho})^2}{4k\delta} \qquad (5.3)$$

Now by combining equations 5.3, 20.0, and 21.0, assuming that $F_{AB} = 1$, and solving for D_o one obtains:

$$D_o = \frac{(g+2)\left(1-\frac{1}{\rho}\right)^2 Q_L}{\eta_f \pi k \lambda \left(1-\left(\frac{1}{\rho}\right)^2\right)\left(1-\left(\frac{T_m}{T_L}\right)^4\right) T_L} \qquad (26.0)$$

From equation 26.0 and the definition of ρ, the expression for D_i is:

$$D_i = \frac{D_o}{\rho} \qquad (27.0)$$

Having computed D_o, given Q_L, T_m, T_L, ρ, λ, η_f, σ, ε, g, and k, it is possible to compute the corresponding value for δ from equation 5.3 as:

$$\delta = \frac{\sigma \varepsilon T_L^3 D_o^2 \left(1 - \frac{1}{\rho}\right)^2}{4k\lambda} \qquad (27.0)$$

Based on the geometry presented in Figure 15 and the foregoing definitions and constraints, the number of rotor disks required is:

$$N_R = \frac{D_o}{2\delta(g+2)} \qquad (28.0)$$

and the number of stator disks is:

$$N_S = N_R + 1 \qquad (28.1)$$

Equations 20.0 and 21.0 can be used to verify the calculations by computing A_m, and Q_L. The relative heat leak can then be computed by using equation 24.0. Appendix I presents the APL computer program that parametrically performs these calculations. Appendix II presents the results of several typical analysis.

In conducting these calculations, it is good practice to use a value for Q_L than is at least 50% greater than the actual cooling load anticipated. For a final design, It is necessary correct the value of δ to correspond to ½ available stock thickness. The actual outside diameter of the rotary disk elements should be about $D_{B_o} = D_o - 4\delta$, and the actual inside diameter of the stator disks should be about $D_{A_i} = D_i + 4\delta$. The inside diameter of the rotor disks will be reduced from D_i by twice the wall thickness of the rotor conducting shaft, and the outside diameter of the stator disks will be increased from D_o by twice the wall thickness of the conducting outside structure of the module.

5.0 ROTARY THERMAL COUPLER MODULE CRITICAL COMPONENT DEMONSTRATION

It has been concluded that the critical technology that needs to be demonstrated is the ability to manufacture a set of module components such as shown in Figure 2. An obvious method to be considered would be to cut the stator half cylinders from bar stock using plunge EDM machining and the rotor using wire EDM machining employing a moving workpiece adapter. For optimum (minimum weight) design, the fins should be tapered. Due to the effect of radial direction of heat flow, the stationary fins attached to the interior cylindrical wall can be thinner than the rotating fins attached to the central shaft for an optimized design.

In principle, the EDM machining approach could provide the capability to make tapered fins. Unfortunately, the tooling for the EDM process would be very expensive, and may not be able to provide the close spacing and the low fin thickness to fin diameter ratio that is required to meet the low relative heat leak goal.

A stacked, bonded sheet metal assembly is a low cost method for demonstrating the technology. This approach can provide both close spacing and the low fin thickness to fin diameter ratio. The core sizing routine outlined in Section 4.0 anticipated this conclusion, hence the reference to stock material thickness. Several alternative fabrication techniques were evaluated. The basic materials considered were limited to Aluminum and Copper. Fabrication techniques considered included soldering, brazing, diffusion bonding, and spin welding.

This phase of the task consumed many man hours, requiring an extensive review of the literature and numerous conversations with potential material suppliers, sheet metal fabricators, and metal bonding job shops.

After all the material, processes, and vendors were surveyed, it was concluded that fabrication of the rotary thermal module elements as vacuum brazed Aluminum parts was the best choice. For this demonstration, a small module was designed which incorporated some self fixturing provisions to simplify the fabrication process. Figures 16 and 17 show graphically summarize the parts details and their assembly process. The parts list for a module was:

Rotary Thermal Coupler Parts List

ITEM	SIZE	MATERIAL	QUANTITY
Rotor Disk	0.50"ID, 3.00"OD	0.010" 3003 Al	40
Stator Disk	1.00"ID, 3.50"OD	0,010" 3003 Al	39
Stator End Disks	1.00"ID, 3.50"OD	0.025" 3003 Al	2
Rotor Spacer	0.50"ID, 0.75"OD	0.020" #8 Braze Sheet	41
Stator Spacer	3.10"OD, 3.50"OD	0.020" #8 Braze Sheet	40
Rotor Stack Tube	1.75" Long	0.50"OD, 0.10" Wall 3003 Al	1

The parts were cut from the sheet stock and the cut edges were deburred. The rotor disks and spacers were assembled on the rotor stack tube. The stator end disks, stator spacers, and stator disks were assembled in a 3 pin assembly braze fixture, the pin spacing defining the stator outside diameter.

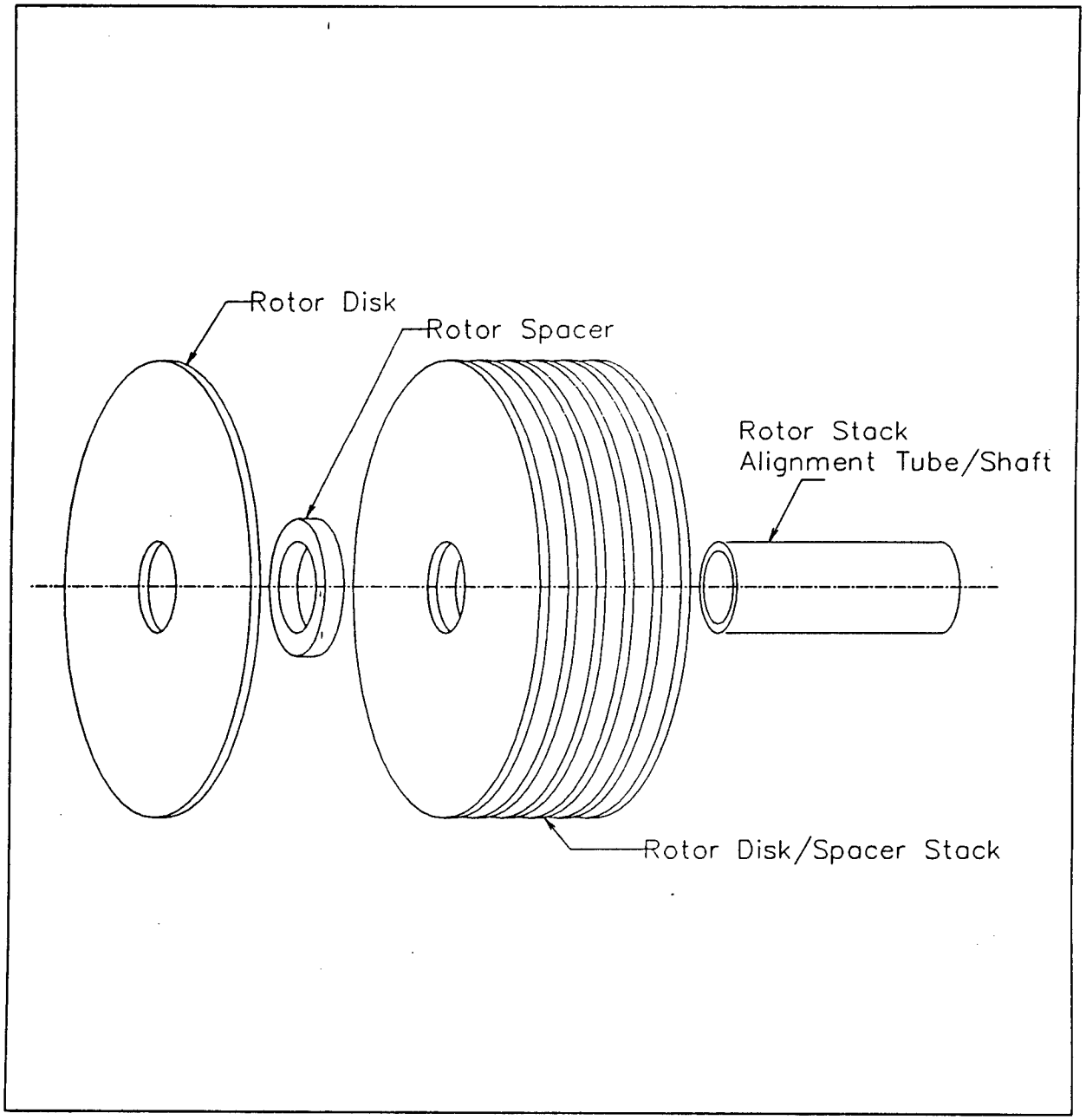

Figure 16 - Rotor Parts and Assembly

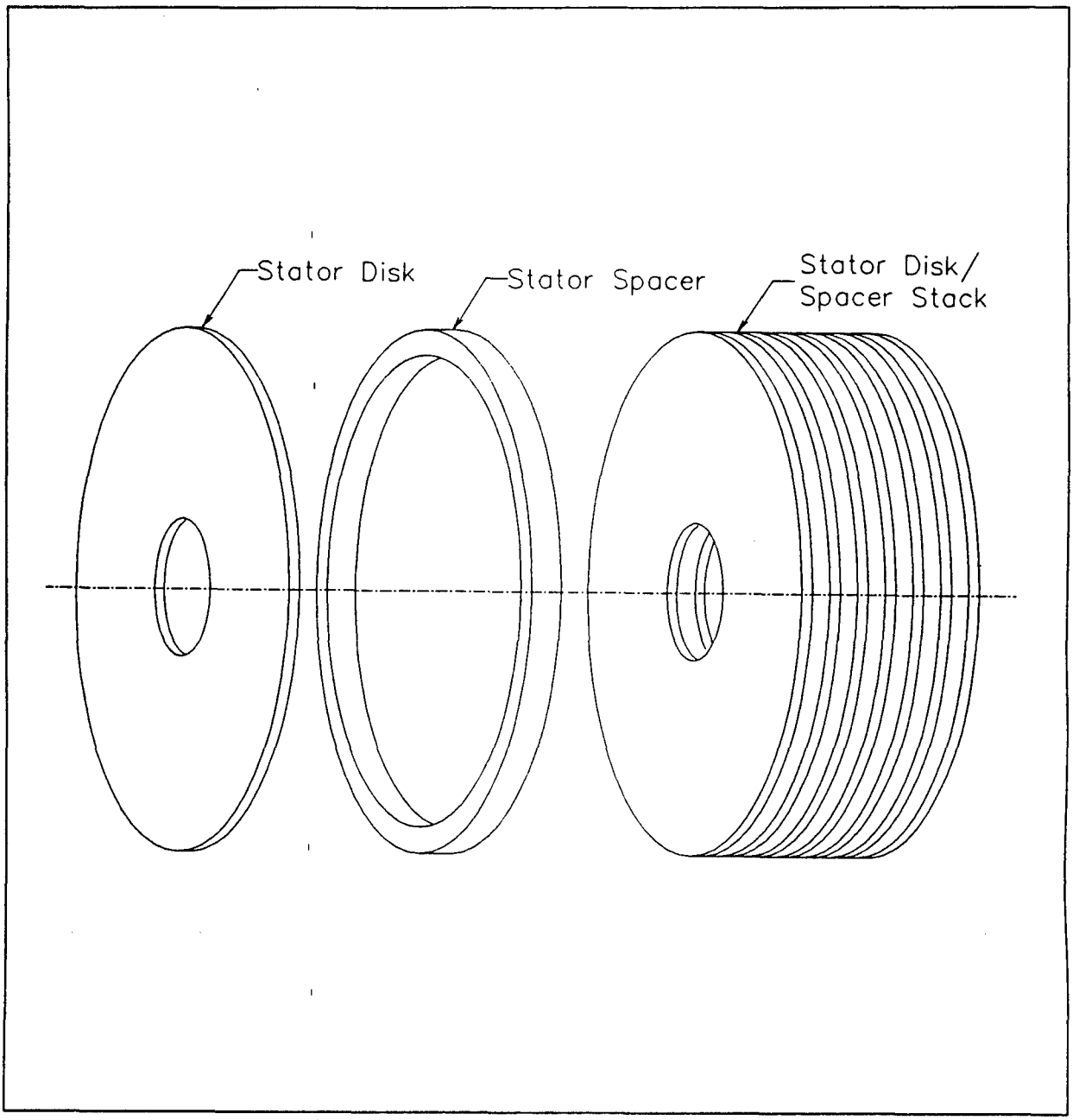

Figure 17 - Stator Parts and Assembly

The two assemblies were placed within specially designed vacuum brazing fixtures, placed within the vacuum furnace, thermocouples were installed to monitor the temperature response of the parts being brazed, and then the parts were vacuum brazed using a temperature-time profile proprietary to the vacuum brazing vendor.

After the successful brazing, the stator was cut diametrically in half. The two stator parts were assembled over the rotor part. Figure 18 presents photographs of the details and the fabricated parts.

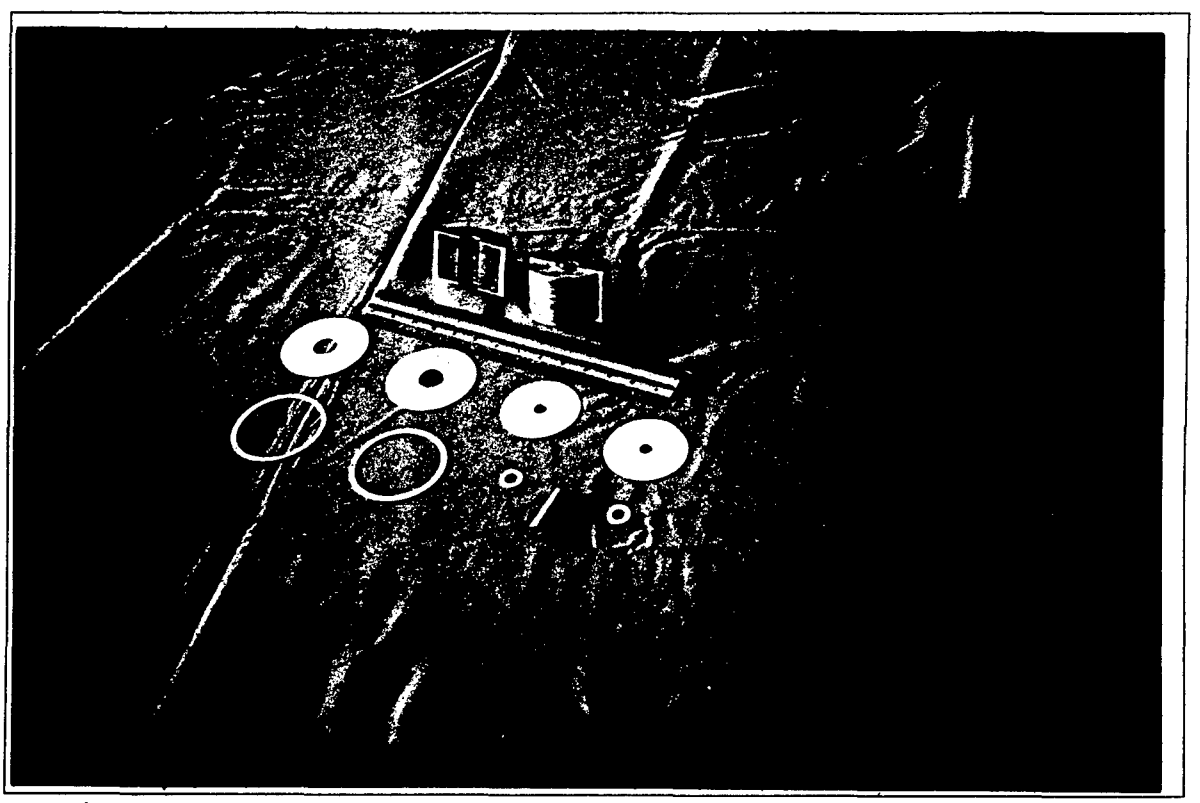

Figure 18 - Photograph of Details and Assemblies

6.0 CONCLUSIONS AND RECOMMENDATIONS

This Phase I effort has developed and demonstrated the principles and practices required for the design and fabrication of a Rotary Cryogenic Thermal Coupling.

A detailed mathematical analysis of the radiant heat transfer occurring within the basic Rotary Cryogenic Thermal Coupling module has been presented, resulting in a mapping of the module disk fin effectiveness versus the disk radius ratio and a component dimensionless characterization parameter, λ, for a specific temperature regime.

An APL computer program has been written to parametriclly size a Rotary Thermal Coupler based on the mathematical analysis developed in this Phase I effort. A listing of the program is presented in Appendix I. A printout of the results of several different cases are presented in Appendix II.

The thermal analysis has demonstrated that the thermal heat leak parasitic losses can be kept within a reasonable percentage of the transferred heat by incorporating active thermal shielding. The technology is applicable down to 10 K.

The preliminary design analysis concluded that the unproven, critical component portion of the Rotary Cryogenic Thermal Coupling was the basic radiation coupled disk assembly. Several alternate materials and processes approaches were considered. It was concluded that a concept based on vacuum brazed Aluminum fabrication was the best option.

A proof of concept module was designed and fabricated. This task demonstrated that the module components could be fabricated. For the purposes of obtaining as much information about this design approach, the fin spacing was selected to be at the extreme minimum value, namely a value of g = 1 was selected, resulting in a nominal clearance of 0.005". This value is now considered to be too close for designs using 3" diameter, 0.010" thick 3003 Aluminum since a slight warpage of either the rotor or the stator disks will result in interference. While the brazed parts initially assembled with adequate clearance to provide for frictionless rotation, subsequent handling has resulted in sufficient distortion of the soft Aluminum parts, thus causing rotor-stator contact. It is possible that this distortion could be removed by reforming the parts using some sort of tooling to straighten out the disks. It is recommended that at this time, however, that a value of g > 2 be used for future initial designs.

A proposal for Phase II was not submitted because there was no formal request issued by the contracting agency. The features which should be considered in such a follow-on effort, nevertheless, were considered. A partial list of such recommended future work should include:

1. Development of an integrated computerized design program.

    A. The design process and the basic kernel of the fin effectiveness program could be melded into an computer program that would output a detailed parts list, given the design heat load and temperature. The program should include an internal table listing the available Aluminum sheet stock.

2. Sources and stocks of Aluminum vacuum brazing sheet should be identified.

A. Although Reynolds Metals Co., Richmond, Virginia manufactures Aluminum vacuum brazing sheet, primarily for the automotive industry, the minimum buy requirement is so great as to virtually eliminate them as a potential source. An intensive search failed to locate any stocking distributors. The material used in the fabrication of the experimental unit was finally obtained as an addendum to an order from a Scandinavian supplier to the vacuum furnace brazing vendor. This is not a satisfactory solution for flight type production hardware.

3. A pair of engineering prototype units should be designed, fabricated, and tested. Figure 19 outlines the recommended testing procedure.

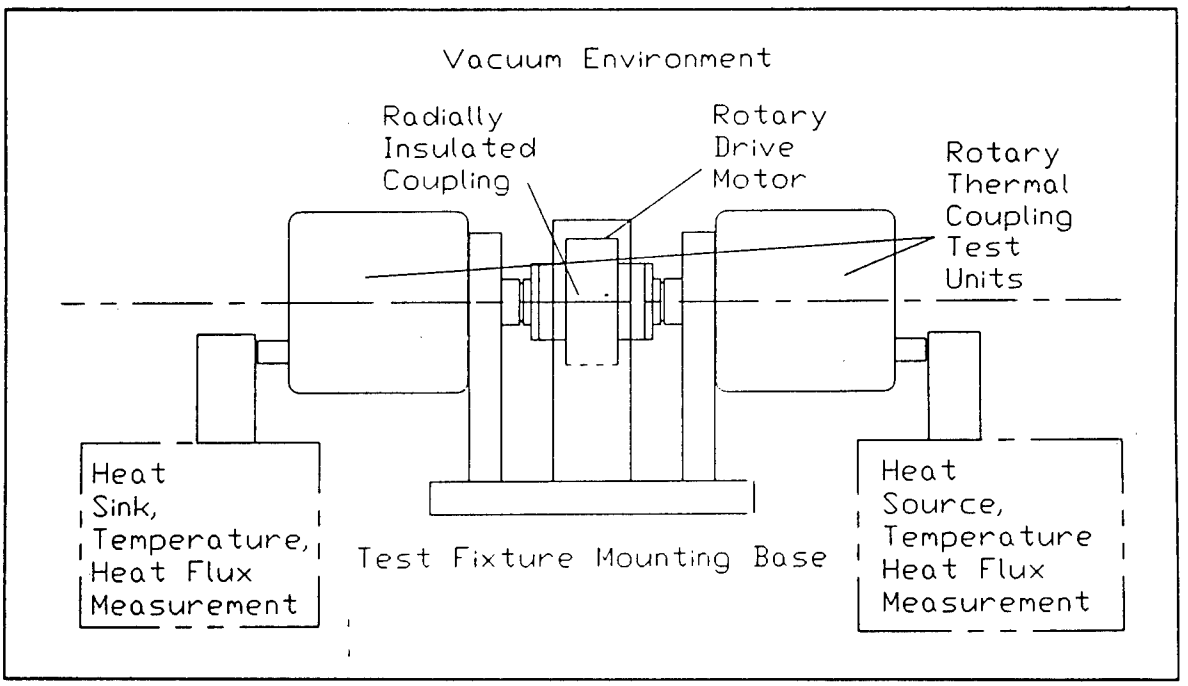

Figure 19 - Rotary Cryogenic Thermal Coupler Test Setup

6.1 POTENTIAL TECHNOLOGY USE

The Rotary Cryogenic Thermal Coupler could prove to be a cost effective component for use on low cost, light weight surveillance satellites to aid in the thermal management of infrared detector systems, optics, and superconducting electronics. The technology is adaptable to higher temperature applications, such as vehicle electronics temperature control and deployable radiator systems when it is desirable to transfer thermal energy across a mechanical joint. A pair of couplers can be assembled to provide effectively a "universal joint" thermal path, thus raising the possibility of eliminating the need to biannually "flip" vehicles which incorporate deep space viewing cryogenic thermal radiators.

Rotary Cryogenic Thermal Couplers could be employed in the medical industry in MRI scanning systems and cryogenic surgery, Such a device could be used to enhance the application of superconducting devices by allowing the relative rotary movement between the cryogenic heat sink (refrigerator or cryogen) and the cryogenic heat source (superconducting device). It could be employed in SQUIB low intensity magnetic field scanning equipment.

7.0 REFERENCES

1. Shaubach, Robert M.; "Rotating Heat Pipe Joint - Design, Fabrication, and Test"; Thermacore, Inc.; AFWAL-TR-83-3053; June 1983
2. Backovsky, Z.F., Rockwell International, Personal Communication,
3. McConnell, B.D., Mecklenburg, K.R.; "Unlubricated Bearing Operation"; Conference on Wear and Lubrication; London; September 1967
4. Mecklenburg, K.R.; "Performance of Ball Bearings in Air and Vacuum With No Added Lubrication"; Midwest Research Institute; Air Force Contract No. F33615-69-C-1236; December 1971
5. Todd, M.J.; "Solid Lubrication of Ball Bearings for Spacecraft Mechanisms"; Tribology International; December 1982
6. Lieblein, S.; "Analysis of Temperature Distribution and Radiant Heat Transfer Along a Rectangular Fin of Constant Thickness"; NASA Technical Note D-196; 1959

8.0 APPENDIX I

```
[0]   RTC
[1]   ⍝ Program sizes a Rotary Thermal Coupler Module
[2]   ⍝ The process is based on that outlined in the
[3]   ⍝ SBIR Phase I Final Report " Rotary Cryogenic
[4]   ⍝ Thermal Coupler", Electro Thermo Associates
[5]   ⍝ 31 October 1996, Dr. A.L. Johnson, P.I.
[6]   'RTCInput'
[7]   RTCInput
[8]   'RTCInitalization'
[9]   RTCInitalization
[10]  'RTCAnalysis'
[11]  RTCAnalysis
[12]  'RTCOutput'
[13]  RTCOutput
```

```
[0]   RTCInput
[1]   ⍝ Function is the input module for the RTC module sizing program. Note that
[2]   ⍝ Copyright, Dr.A.L. Johnson, 1996
[3]   'Input module for the Rotary Thermal Coupler design program. Note that the'
[4]   'program accepts vector strings for the Radius Ratio and the Lamda input'
[5]   'terms, which expedits parametric studies.  The terms in the vector strings'
[6]   'are to be seperated by spacebar blanks. Due to printout limitations, the vector'
[7]   'length of the Radius Ratio parameter is limited to 6 quantities.'
[8]   ' '
[9]   L1:QL←⍎IN 'Enter the design heat load, including margin, 0.01 < QL < 20 watts;
[10]  →((QL<0.01)∨(QL>20))/L1
[11]  L2:TL←⍎IN 'Enter the heat source temperature, at the RTC junction, 5K < TL < 500K;
[12]  →((TL<5)∨(TL>500))/L2
[13]  L3:Tm←⍎IN 'Enter the heat sink temperature at the RTC interface, 4K < Tm < (Tl-1);
[14]  →((Tm<4)∨(Tm≥(TL-1)))/L3
[15]  LA:Tamb←⍎IN 'Enter the ambient environment temperature, TL < Tamb < 500K    '
[16]  →((Tamb<TL)∨(Tamb>500))/LA
[17]  ⍝ L4:Δ←⍎IN 'Enter the disk thickness, Δ, in mm, 0.1mm < Δ < 1mm;    '
[18]  ⍝ →((Δ<0.1)∨(Δ>1))/L4
[19]  L5:K←⍎IN 'Enter the disk thermal conductivity, k - watts/cm.K;  '
[20]  →((K≤0.001)∨(K>100))/L5
[21]  L6:g←⍎IN 'Enter the disk gap factor, g, where gΔ=gap, 1 ≤ g ≤ 5;    '
[22]  →((g<1)∨(g>5))/L6
[23]  L7:mv←(⍳0),mv←⍎IN 'Enter the Module Radius Ratio Vector, 1.5 < ρ = D0/Di < 10;    '
[24]  →(+/((mv<1.01)∨(mv>15')))/L7
[25]  →((⍴mv)>6)/L0
[26]  L8:Lv←(⍳0),Lv←⍎IN 'Enter the Lamda parameter vector, 0.0001 < ι < 1  - '
[27]  →(+/((Lv<0.0001)∨(Lv>1)))/L8
[28]  ⍝ L9:n←⍎IN 'Enter the number of numerical integration steps, 10 < n < 1000;    '
[29]  ⍝ →((n<10)∨(n>1000))/L9
[30]  →End
[31]  L0:'Program linits the allowable number of terms in the ρ vector to 6'
[32]  →L7
[33]  End:
```

```
[0]   RTCInitalization;X;Y
[1]   ⍝ Function establishes the initial conditions for the RTC analysis.
[2]   n←300
[3]   sigma←5.67E¯12 ⍝'Steffan Boltzman constant, Watts/sq.cm-K*4
[4]   TAi←TL ⍝ K
[5]   m←mv[1]
[6]   em←0.85
[7]   esem←0.03
[8]   DsDo←1.25
[9]   TsTm←Tamb÷Tm
[10]  DsDe←1.1
[11]  L←Lv[1]
[12]  X←.01,(0.1×(⍳10))
[13]  Y←0.475,0.5125,0.5625,0.65,0.76,0.89,1.035,1.185,1.34,1.51,1.65
[14]  Co←Y⌹X∘.*((⍳⍴X)-1) ⋄ ⍝ coefficients for ⍳ power series for U0ref
[15]  R←0
[16]  S1ref←S0←Tm÷TL ⋄ ⍝ establishes initial S0 and final S1 values
[17]  T0←1
[18]  U0←U0ref
[19]  V0←0
[20]  QsQlv←Div←Dov←Δv←Amv←QLv←Nv←W0←WN←Nf←M←⍳0
[21]  Wio←Wn←S0,T0,U0,V0
[22]  dR←1÷n
[23]  k←1
[24]  j←1
```

```
[0]   Result←U0ref;a;b;c
[1]   S1T1←2×S0ref*(+/Co×(L*0.5)*((⍳⍴Co)-1))
[2]   Result←¯10E¯6⌊(m-1)×(S1T1-(1+S0ref))÷(ωm)
```

```
[0]   RungeKutta;K1;K2;K3;K4
[1]   ⍝ Function runs 4th order Runge-Kutta numerical analysis
[2]   W←Wn
[3]   K1←dR×dWdR
[4]   R←R+(dR÷2)
[5]   W←Wn+(K1÷2)
[6]   K2←dR×dWdR
[7]   W←Wn+(K2÷2)
[8]   K3←dR×dWdR
[9]   R←R+(dR÷2)
[10]  W←Wn+K3
[11]  K4←dR×dWdR
[12]  Wn←Wn+((K1+(2×K2)+(2×K3)+K4)÷6)
```

```
[0]   RTCAnalysis;cf;nf;Do;ΔΔ;Nn;Am;ql;QsQl;A;B
[1]   ⍝ Function solves the Rotary Thermal Coupler differential equations
[2]   'ι, lamda; ρ=Do/Di; Iterations'
[3]   L2:M←M,Wn
[4]   RungeKutta ◊ ⍝ Function runs 4th order RungeKutta numerical analysis
[5]   →(R<1)/L2
[6]   →((Wn[4]≤0)∧(((|(m-(U0÷Wn[4])))×10E5)<5))/L3
[7]   U0←(U0-((Wn[3]×2÷(1?5))))
[8]   cf←(1?9)÷20
[9]   U0←(U0+(cf×((m-1)÷⍟m)×((Wn[1]+Wn[2])-(1+S0))))÷(1+cf)
[10]  R←0
[11]  Wn←S0,T0,U0,V0
[12]  Wi←Wn ◊ M←ι0
[13]  j←j+1
[14]  →(j≥800)/L7
[15]  →L2
[16]  L3:ΔS0←S1ref-Wn[1]
[17]  ΔS0←(1-(L÷(1+(1?5))))×ΔS0
[18]  →((|(ΔS0÷S1ref))<10E¯5)/L4
[19]  S0←S0+ΔS0
[20]  →((S0≤0)∨(S0≥1))/L6
[21]  →L2
[22]  L4:Wi←M[1],M[2],M[3],M[4]
[23]  M←M,Wn ◊ W0←W0,Wi
[24]  WN←WN,Wn
[25]  Nf←Nf,nf←-((2×Wi[3])÷(L×(m+1)×(1-(Wn[1]⋆4))))
[26]  Do←(QL×(g+2)×((1-(1÷m))⋆2))÷(nf×TL×(1-((Tm÷TL)⋆4))×o1×(1-((1÷m)⋆2))×K×L)
[27]  Dov←Dov,Do ◊ Div←Div,(Do÷m)
[28]  Δv←Δv,ΔΔ←(sigma×em×(TL⋆3)×(Do⋆2)×((1-(1÷m))⋆2))÷(4×K×L)
[29]  Amv←Amv,Am←(o1×(1-((1÷m)⋆2))×(Do⋆3))÷(4×(g+2)×ΔΔ)
[30]  QLv←QLv,ql←(nf×Am×sigma×em×((TL⋆4)-(Tm⋆4)))
[31]  Nv←Nv,Nn←Do÷((g+2)×ΔΔ)
[32]  QsQl←6×esem×(g+2)×ΔΔ×((DsDo)⋆2)×(((TsTm)⋆4)-1)÷Do
[33]  QsQl←QsQl÷(nf×(1+(DsDe⋆2))×4×(1-((1÷m)⋆2))×(((TL÷Tm)⋆4)-1))
[34]  QsQlv←QsQlv,QsQl
[35]  (8 6⍕L),(8 3⍕m),(8 0⍕j)
[36]  L6:M←ι0 ◊ j←1 ◊ i←Lvι1L
[37]  →(i=ρLv)/L7
[38]  i←i+1
[39]  L←Lv[i]
[40]  U0←U0ref ◊ S0←S1ref
[41]  Wn←S0,T0,U0,V0
[42]  →L2
[43]  L7:i←mvιm
[44]  →(i=ρmv)/End
[45]  i←i+1
[46]  m←mv[i] ◊ L←Lv[1]
[47]  U0←U0ref ◊ S0←S1ref
[48]  Wn←S0,T0,U0,V0
[49]  →L2
[50]  End:
```

```
[0]   Result←dWdR;dSdR;dTdR;dUdR;dVdR;S;T;U;V
[1]   ⍝ The derivitives defined above are used to compute the
[2]   ⍝ parameters required by the Runge-Kutta numerical process
[3]   ⍝ Input is the vector of system dependent variables
[4]   ⍝ existing at the dependent variable R. Output is the
[5]   ⍝ vector of the system dependent variable deratives at R.
[6]   S←0⌈W[1] ⋄ T←0⌈W[2] ⋄ U←0⌊W[3] ⋄ V←0⌊W[4]
[7]   dSdR←V
[8]   dTdR←U
[9]   dUdR←(L×((T*4)-(S*4)))-(U÷(R+(1÷(m-1))))
[10]  dVdR←(¯1)×((L×((T*4)-(S*4)))+(V÷(R+(1÷(m-1)))))
[11]  Result←dSdR,dTdR,dUdR,dVdR
```

```
[0]   RTCOutput
[1]   InputDataFile
[2]   FinEffectivenessOutput
[3]   OutsideDiameterOutput
[4]   InsideDiameterOutput
[5]   DiskThicknessOutput
[6]   HeatLeakParameterOutput
[7]   RotorStatorDiskSpacerOutput
[8]   RotorDiskCountOutput
[9]   StatorDiskCountOutput
[10]  ClearWorkSpaceVariables
```

```
[0]   InputDataFile;A
[1]   ' '
[2]   A←' Heat Load ',(4 2⍕QL),' watts; Source temp., TL, '
[3]   A←A,(6 2⍕TL),' K; Sink temp., Tm,',(5 2⍕Tm),'K'
[4]   A
[5]   ' '
[6]   A←'Ambient Temp., Tamb,'(6 2⍕Tamb)
[7]   A←A,'K; Thermal conductivity, k,',(5 2⍕K),' watts/cm.K'
[8]   A
[9]   ' '
[10]  A←' Disk Gap Factor, g = ',(3 1⍕g)
[11]  A←A,'; Number of numerical intergration steps, n =',(5 0⍕n)
[12]  A
[13]  ' '
```

```
[0]   ClearWorkSpaceVariables
[1]   ⎕ERASE  'Am DsDe Nf QsQlv TAi Ustart Wio g n ΔT Amv DsDo Nn R TL V0 esem'
[2]   ⎕ERASE  'Wn i nf Δv Co K Nv S0 Tamb W cf j ql ΔΔ Div L QL S1T1 Tm W0 mv'
[3]   ⎕ERASE  'Lv QLv S1ref TsTm WN em m Δ dR k sigma Do Dov M QsQl T0 U0 Wi ΔS0'
```

```
[0]   FinEffectivenessOutput;Column;Space;Row;Data;output
[1]   Column←10 3⍕mv
[2]   Space←('    ⍳ \')⍪((⍴Column)⍴' ')
[3]   Column←('    \ ⍴')⍪Column
[4]   Row←((⍴Lv), 7)⍴(7 5⍕Lv)
[5]   Data←⍉(((⍴mv),(⍴Lv))⍴Nf)
[6]   output←Row⍪[2](10 3⍕Data)
[7]   '            ⍴ = r0/ri, lambda - ⍳, versus radiation fin effectiveness'
[8]   ' '
[9]   Column⍪(Space⍪output)


[0]   InsideDiameterOutput;Column;Space;Row;Data;output
[1]   Column←10 3⍕mv
[2]   Space←('    ⍳ \')⍪((⍴Column)⍴' ')
[3]   Column←('    \ ⍴')⍪Column
[4]   Row←((⍴Lv), 7)⍴(7 5⍕Lv)
[5]   Data←⍉(((⍴mv),(⍴Lv))⍴(Div))
[6]   output←Row⍪[2](10 3⍕Data)
[7]   ' '
[8]   '            ⍴ = r0/ri, lambda - ⍳, versus radiation disk ID - cm.'
[9]   ' '
[10]  Column⍪(Space⍪output)


[0]   OutsideDiameterOutput;Column;Space;Row;Data;output
[1]   Column←10 3⍕mv
[2]   Space←('    ⍳ \')⍪((⍴Column)⍴' ')
[3]   Column←('    \ ⍴')⍪Column
[4]   Row←((⍴Lv), 7)⍴(7 5⍕Lv)
[5]   Data←⍉(((⍴mv),(⍴Lv))⍴Dov)
[6]   output←Row⍪[2](10 3⍕Data)
[7]   ' '
[8]   '            ⍴ = r0/ri, lambda - ⍳, versus radiation disk OD - cm.'
[9]   ' '
[10]  Column⍪(Space⍪output)


[0]   DiskThicknessOutput;Column;Space;Row;Data;output
[1]   Column←10 3⍕mv
[2]   Space←('    ⍳ \')⍪((⍴Column)⍴' ')
[3]   Column←('    \ ⍴')⍪Column
[4]   Row←((⍴Lv), 7)⍴(7 5⍕Lv)
[5]   Data←⍉(((⍴mv),(⍴Lv))⍴(20×Δv))
[6]   output←Row⍪[2](10 3⍕Data)
[7]   ' '
[8]   '            ⍴ = r0/ri, lambda - ⍳, versus radiation disk thickness - mm.'
[9]   ' '
[10]  Column⍪(Space⍪output)
```

```
[0]   HeatLeakParameterOutput;Column;Space;Row;Data;output
[1]   Column←10 3⍕mv
[2]   Space←('    ⍳ \')⍪((⍴Column)⍴' ')
[3]   Column←('    \ ⍴')⍪Column
[4]   Row←((⍴Lv), 7)⍴(7 5⍕Lv)
[5]   Data←⍉(((⍴mv),(⍴Lv))⍴(QsQlv))
[6]   output←Row⍪[2](10 4⍕Data)
[7]   ' '
[8]   '            ⍴ = r0/ri, lambda - ⍳, versus Heat Leak Parameter, Qs/QL '
[9]   ' '
[10]  Column⍪(Space⍪output)


[0]   RotorStatorDiskSpacerOutput;Column;Space;Row;Data;output
[1]   Column←10 3⍕mv
[2]   Space←('    ⍳ \')⍪((⍴Column)⍴' ')
[3]   Column←('    \ ⍴')⍪Column
[4]   Row←((⍴Lv), 7)⍴(7 5⍕Lv)
[5]   Data←⍉(((⍴mv),(⍴Lv))⍴(20×Δv×(1+g)))
[6]   output←Row⍪[2](10 3⍕Data)
[7]   ' '
[8]   '            ⍴ = r0/ri, lambda - ⍳, versus Rotor/Stator Stack Spacing   mm'
[9]   ' '
[10]  Column⍪(Space⍪output)


[0]   RotorDiskCountOutput;Column;Space;Row;Data;output
[1]   Column←10 3⍕mv
[2]   Space←('    ⍳ \')⍪((⍴Column)⍴' ')
[3]   Column←('    \ ⍴')⍪Column
[4]   Row←((⍴Lv), 7)⍴(7 5⍕Lv)
[5]   Data←⍉(((⍴mv),(⍴Lv))⍴(⌈(Nv÷2)))
[6]   output←Row⍪[2](10 0⍕Data)
[7]   ' '
[8]   '            ⍴ = r0/ri, lambda - ⍳, versus number of rotor disks '
[9]   ' '
[10]  Column⍪(Space⍪output)


[0]   StatorDiskCountOutput;Column;Space;Row;Data;output
[1]   Column←10 3⍕mv
[2]   Space←('    ⍳ \')⍪((⍴Column)⍴' ')
[3]   Column←('    \ ⍴')⍪Column
[4]   Row←((⍴Lv), 7)⍴(7 5⍕Lv)
[5]   Data←⍉(((⍴mv),(⍴Lv))⍴(1+⌈(Nv÷2)))
[6]   output←Row⍪[2](10 0⍕Data)
[7]   ' '
[8]   '            ⍴ = r0/ri, lambda - ⍳, versus number of Stator disks '
[9]   ' '
[10]  Column⍪(Space⍪output)
```

9.0 APPENDIX II

RTC

RTCInput

Input module for the Rotary Thermal Coupler design program. Note that the program accepts vector strings for the Radius Ratio and the Lamda input terms, which expedits parametric studies. The terms in the vector strings are to be seperated by commas. Due to printout limitations, the vector length of the Radius Ratio parameter is limited to 6 quantities.

Enter the design heat load, including margin, 0.01 < QL < 20 watts; 1

Enter the heat source temperature, at the RTC junction, 5K < TL < 500K; 65

Enter the heat sink temperature at the RTC interface, 4K < Tm < (Tl-1); 60

Enter the ambient environment temperature, TL < Tamb < 500K 250

Enter the disk thermal conductivity, k - watts/cm.K; 2.5

Enter the disk gap factor, g, where g=gap, 1 ≤ g ≤ 5; 2

Enter the Module Radius Ratio Vector, 1.5 < ρ = D0/Di < 10; 1.5,3,6,10

Enter the Lamda parameter vector, 0.0001 < ι < 1 - (.01,.02,.05,.1,.15,(.1+(.1×19)))*2

RTCInitalization

RTCAnalysis

Heat Load 1.00 watts; Source temp., TL, 65.00 K; Sink temp., Tm,60.00K

Ambient Temp., Tamb, 250.00 K; Thermal conductivity, k, 2.50 watts/cm.K

Disk Gap Factor, g = 2.0; Number of numerical intergration steps, n = 300

ρ = r0/ri, lambda - ι, versus radiation fin effectiveness

ι \ ρ	1.500	3.000	6.000	10.000
0.0001	1.000	1.000	1.000	1.000
0.0004	0.999	0.999	0.999	0.998
0.0025	0.994	0.993	0.991	0.989
0.0100	0.976	0.971	0.965	0.958
0.0225	0.947	0.938	0.924	0.911
0.0400	0.910	0.895	0.873	0.853
0.0900	0.818	0.793	0.755	0.724
0.1600	0.717	0.685	0.638	0.599
0.2500	0.621	0.585	0.533	0.493
0.3600	0.533	0.497	0.446	0.406
0.4900	0.458	0.423	0.374	0.337
0.6400	0.394	0.362	0.317	0.283
0.8100	0.341	0.311	0.270	0.239
1.0000	0.296	0.270	0.232	0.205

ρ = r0/ri, lambda - ι, versus radiation disk OD - cm.

ι \ ρ	1.500	3.000	6.000	10.000
0.0001	57.212	143.036	204.352	234.091
0.0004	14.314	35.791	51.144	58.600
0.0025	2.302	5.762	8.246	9.462
0.0100	0.586	1.472	2.118	2.442
0.0225	0.268	0.678	0.983	1.141
0.0400	0.157	0.399	0.585	0.686
0.0900	0.078	0.200	0.300	0.359
0.1600	0.050	0.130	0.200	0.244
0.2500	0.037	0.098	0.153	0.190
0.3600	0.030	0.080	0.127	0.160
0.4900	0.025	0.069	0.111	0.142
0.6400	0.023	0.062	0.101	0.129
0.8100	0.021	0.057	0.093	0.121
1.0000	0.019	0.053	0.088	0.114

ρ = r0/ri, lambda - ι, versus radiation disk ID - cm.

ι \ ρ	1.500	3.000	6.000	10.000
0.0001	38.141	47.679	34.059	23.409
0.0004	9.542	11.930	8.524	5.860
0.0025	1.535	1.921	1.374	0.946
0.0100	0.391	0.491	0.353	0.244
0.0225	0.179	0.226	0.164	0.114
0.0400	0.105	0.133	0.098	0.069
0.0900	0.052	0.067	0.050	0.036
0.1600	0.033	0.043	0.033	0.024
0.2500	0.025	0.033	0.026	0.019
0.3600	0.020	0.027	0.021	0.016
0.4900	0.017	0.023	0.019	0.014
0.6400	0.015	0.021	0.017	0.013
0.8100	0.014	0.019	0.016	0.012
1.0000	0.013	0.018	0.015	0.011

ρ = r0/ri, lambda - ι, versus radiation disk thickness - mm.

ι \ ρ	1.500	3.000	6.000	10.000
0.0001	9.627	240.702	767.655	1174.974
0.0004	0.151	3.768	12.021	18.407
0.0025	0.001	0.016	0.050	0.077
0.0100	0.000	0.000	0.001	0.001
0.0225	0.000	0.000	0.000	0.000
0.0400	0.000	0.000	0.000	0.000
0.0900	0.000	0.000	0.000	0.000
0.1600	0.000	0.000	0.000	0.000
0.2500	0.000	0.000	0.000	0.000
0.3600	0.000	0.000	0.000	0.000
0.4900	0.000	0.000	0.000	0.000
0.6400	0.000	0.000	0.000	0.000
0.8100	0.000	0.000	0.000	0.000
1.0000	0.000	0.000	0.000	0.000

ρ = r0/ri, lambda - ι, versus Heat Leak Parameter, Qs/QL

ι \ ρ	1.500	3.000	6.000	10.000
0.0001	1.5347	9.5927	19.5797	25.6933
0.0004	0.0961	0.6006	1.2264	1.6100
0.0025	0.0025	0.0156	0.0319	0.0420
0.0100	0.0002	0.0010	0.0021	0.0028
0.0225	0.0000	0.0002	0.0005	0.0006
0.0400	0.0000	0.0001	0.0002	0.0002
0.0900	0.0000	0.0000	0.0000	0.0001
0.1600	0.0000	0.0000	0.0000	0.0000
0.2500	0.0000	0.0000	0.0000	0.0000
0.3600	0.0000	0.0000	0.0000	0.0000
0.4900	0.0000	0.0000	0.0000	0.0000
0.6400	0.0000	0.0000	0.0000	0.0000
0.8100	0.0000	0.0000	0.0000	0.0000
1.0000	0.0000	0.0000	0.0000	0.0000

ρ = r0/ri, lambda - ι, versus Rotor/Stator Stack Spacing mm

ι \ ρ	1.500	3.000	6.000	10.000
0.0001	28.882	722.105	2302.966	3524.921
0.0004	0.452	11.303	36.064	55.221
0.0025	0.002	0.047	0.150	0.230
0.0100	0.000	0.001	0.002	0.004
0.0225	0.000	0.000	0.000	0.000
0.0400	0.000	0.000	0.000	0.000
0.0900	0.000	0.000	0.000	0.000
0.1600	0.000	0.000	0.000	0.000
0.2500	0.000	0.000	0.000	0.000
0.3600	0.000	0.000	0.000	0.000
0.4900	0.000	0.000	0.000	0.000
0.6400	0.000	0.000	0.000	0.000
0.8100	0.000	0.000	0.000	0.000
1.0000	0.000	0.000	0.000	0.000

ρ = r0/ri, lambda - ι, versus number of rotor disks

ι \ ρ	1.500	3.000	6.000	10.000
0.0001	15	2	1	1
0,0004	238	24	11	8
0.0025	9231	922	413	309
0.0100	144988	14435	6422	4776
0.0225	712378	70565	31139	22988
0.0400	2162582	212836	92975	68023
0.0900	9844698	954507	407409	292143
0.1600	27295645	2607049	1087364	764728
0.2500	57636064	5432003	2219775	1535098
0.3600	102697103	9574349	3846821	2623567
0.4900	163361787	15098701	5983707	4035828
0.6400	239837234	22026497	8634457	5771795
0.8100	332183946	30355956	11798640	7829863
1.0000	440301190	40088133	15473540	10212739

```
     RTC
RTCInput
Input module for the Rotary Thermal Coupler design program. Note that the
program accepts vector strings for the Radius Ratio and the Lamda input
terms, which expedits parametric studies.  The terms in the vector strings
are to be seperated by commas. Due to printout limitations, the vector
length of the Radius Ratio parameter is limited to 6 quantities.

Enter the design heat load, including margin, 0.01 < QL < 20 watts;     1

Enter the heat source temperature, at the RTC junction, 5K < TL < 500K;    65

Enter the heat sink temperature at the RTC interface, 4K < Tm < (Tl-1);    60

Enter the ambient environment temperature, TL < Tamb < 500K    250

Enter the disk thermal conductivity, k - watts/cm.K;  2.5

Enter the disk gap factor, g, where g=gap, 1 ≤ g ≤ 5;    2

Enter the Module Radius Ratio Vector, 1.5 < ρ = D0/Di < 10;    3.5

Enter the Lamda parameter vector, 0.0001 < ι < 1  - 0.0013,0.00135,0.0014

RTCInitalization
RTCAnalysis
ι, lamda; ρ=Do/Di; Iterations
0.001300    3.500       97
0.001350    3.500      103
0.001400    3.500       85

 Heat Load 1.00 watts; Source temp., TL,  65.00 K; Sink temp., Tm,60.00K

 Ambient Temp., Tamb, 250.00 K; Thermal conductivity, k, 2.50 watts/cm.K

 Disk Gap Factor, g = 2.0; Number of numerical intergration steps, n =  300

             ρ = r0/ri, lambda - ι, versus radiation fin effectiveness

    \ ρ      3.500
    ι \
0.00130      0.996
0.00135      0.996
0.00140      0.996

             ρ = r0/ri, lambda - ι, versus radiation disk OD - cm.

    \ ρ      3.500
    ι \
0.00130     12.271
0.00135     11.818
0.00140     11.398
```

ρ = r0/ri, lambda - ι, versus radiation disk ID - cm.

\ ρ ι \	3.500
0.00130	3.506
0.00135	3.377
0.00140	3.257

ρ = r0/ri, lambda - ι, versus radiation disk thickness - mm.

\ ρ ι \	3.500
0.00130	0.156
0.00135	0.140
0.00140	0.125

ρ = r0/ri, lambda - ι, versus Heat Leak Parameter, Qs/QL

\ ρ ι \	3.500
0.00130	0.0706
0.00135	0.0655
0.00140	0.0609

ρ = r0/ri, lambda - ι, versus Rotor/Stator Stack Spacing mm

\ ρ ι \	3.500
0.00130	0.469
0.00135	0.419
0.00140	0.376

ρ = r0/ri, lambda - ι, versus number of rotor disks

\ ρ ι \	3.500
0.00130	197
0.00135	212
0.00140	228

ρ = r0/ri, lambda - ι, versus number of Stator disks

\ ρ ι \	3.500
0.00130	198
0.00135	213
0.00140	229

```
    RTC
RTCInput
Input module for the Rotary Thermal Coupler design program. Note that the
program accepts vector strings for the Radius Ratio and the Lamda input
terms, which expedits parametric studies.  The terms in the vector strings
are to be seperated by spacebar blanks. Due to printout limitations, the vector
length of the Radius Ratio parameter is limited to 6 quantities.

Enter the design heat load, including margin, 0.01 < QL < 20 watts;     .35

Enter the heat source temperature, at the RTC junction, 5K < TL < 500K;   40

Enter the heat sink temperature at the RTC interface, 4K < Tm < (Tl-1);   35

Enter the ambient environment temperature, TL < Tamb < 500K   120

Enter the disk thermal conductivity, k - watts/cm.K;  2.5

Enter the disk gap factor, g, where g^=gap, 1 ≤ g ≤ 5;   2

Enter the Module Radius Ratio Vector, 1.5 < ρ = D0/Di < 10;   3,3.5,4,4.5

Enter the Lamda parameter vector, 0.0001 < ι < 1  - .00035,.00055,.00075,.001,.0015,.002

RTCInitalization
RTCAnalysis
 Heat Load 0.35 watts; Source temp., TL,  40.00 K; Sink temp., Tm,35.00K

 Ambient Temp., Tamb, 120.00 K; Thermal conductivity, k, 2.50 watts/cm.K

 Disk Gap Factor, g = 2.0; Number of numerical intergration steps, n =  300

            ρ = r0/ri, lambda - ι, versus radiation fin effectiveness

    \ ρ      3.000     3.500     4.000     4.500
    ι \
0.00035      0.999     0.999     0.999     0.999
0.00055      0.998     0.998     0.998     0.998
0.00075      0.998     0.998     0.998     0.998
0.00100      0.997     0.997     0.997     0.997
0.00150      0.996     0.996     0.995     0.995
0.00200      0.994     0.994     0.994     0.994

            ρ = r0/ri, lambda - ι, versus radiation disk OD - cm.

    \ ρ      3.000     3.500     4.000     4.500
    ι \
0.00035     15.399    17.111    18.481    19.602
0.00055      9.805    10.896    11.768    12.482
0.00075      7.195     7.995     8.635     9.160
0.00100      5.400     6.001     6.482     6.875
0.00150      3.605     4.006     4.328     4.591
0.00200      2.708     3.009     3.251     3.449
```

ρ = r0/ri, lambda - ι, versus radiation disk ID - cm.

ι \ ρ	3.000	3.500	4.000	4.500
0.00035	5.133	4.889	4.620	4.356
0.00055	3.268	3.113	2.942	2.774
0.00075	2.398	2.284	2.159	2.035
0.00100	1.800	1.714	1.620	1.528
0.00150	1.202	1.145	1.082	1.020
0.00200	0.903	0.860	0.813	0.766

ρ = r0/ri, lambda - ι, versus radiation disk thickness - mm.

ι \ ρ	3.000	3.500	4.000	4.500
0.00035	0.186	0.263	0.339	0.410
0.00055	0.048	0.068	0.087	0.106
0.00075	0.019	0.027	0.035	0.042
0.00100	0.008	0.011	0.015	0.018
0.00150	0.002	0.003	0.004	0.005
0.00200	0.001	0.001	0.002	0.002

ρ = r0/ri, lambda - ι, versus Heat Leak Parameter, Qs/QL

ι \ ρ	3.000	3.500	4.000	4.500
0.00035	0.0168	0.0207	0.0242	0.0272
0.00055	0.0068	0.0084	0.0098	0.0110
0.00075	0.0037	0.0045	0.0053	0.0059
0.00100	0.0021	0.0026	0.0030	0.0033
0.00150	0.0009	0.0011	0.0013	0.0015
0.00200	0.0005	0.0006	0.0007	0.0008

ρ = r0/ri, lambda - ι, versus Rotor/Stator Stack Spacing mm

ι \ ρ	3.000	3.500	4.000	4.500
0.00035	0.557	0.790	1.016	1.229
0.00055	0.144	0.204	0.262	0.317
0.00075	0.057	0.080	0.104	0.125
0.00100	0.024	0.034	0.044	0.053
0.00150	0.007	0.010	0.013	0.016
0.00200	0.003	0.004	0.006	0.007

ρ = r0/ri, lambda - ι, versus number of rotor disks

ι \ ρ	3.000	3.500	4.000	4.500
0.00035	208	163	137	120
0.00055	512	401	337	296
0.00075	951	746	626	549
0.00100	1689	1324	1112	975
0.00150	3794	2974	2498	2189
0.00200	6736	5279	4433	3885

RTC

RTCInput
Input module for the Rotary Thermal Coupler design program. Note that the program accepts vector strings for the Radius Ratio and the Lamda input terms, which expedits parametric studies. The terms in the vector strings are to be seperated by spacebar blanks. Due to printout limitations, the vector length of the Radius Ratio parameter is limited to 6 quantities.

Enter the design heat load, including margin, 0.01 < QL < 20 watts; .15

Enter the heat source temperature, at the RTC junction, 5K < TL < 500K; 12

Enter the heat sink temperature at the RTC interface, 4K < Tm < (Tl-1); 10

Enter the ambient environment temperature, TL < Tamb < 500K 60

Enter the disk thermal conductivity, k - watts/cm.K; 1

Enter the disk gap factor, g, where gΔ=gap, 1 ≤ g ≤ 5; 2

Enter the Module Radius Ratio Vector, 1.5 < ρ = D0/Di < 10; 3 4 5

Enter the Lamda parameter vector, 0.0001 < ι < 1 - .0002,.0003,.0004,.0005

RTCInitalization
RTCAnalysis
Heat Load 0.15 watts; Source temp., TL, 12.00 K; Sink temp., Tm,10.00K

Ambient Temp., Tamb, 60.00 K; Thermal conductivity, k, 1.00 watts/cm.K

Disk Gap Factor, g = 2.0; Number of numerical intergration steps, n = 300

ρ = r0/ri, lambda - ι, versus radiation fin effectiveness

ι \ ρ	3.000	4.000	5.000
0.00020	0.999	0.999	0.999
0.00030	0.999	0.999	0.999
0.00040	0.999	0.999	0.999
0.00050	0.999	0.998	0.998

ρ = r0/ri, lambda - ι, versus radiation disk OD - cm.

ι \ ρ	3.000	4.000	5.000
0.00020	76.893	92.277	102.535
0.00030	51.276	61.537	68.379
0.00040	38.468	46.167	51.301
0.00050	30.783	36.945	41.055

ρ = r0/ri, lambda - ι, versus radiation disk ID - cm.

ι \ ρ	3.000	4.000	5.000
0.00020	25.631	23.069	20.507
0.00030	17.092	15.384	13.676
0.00040	12.823	11.542	10.260
0.00050	10.261	9.236	8.211

ρ = r0/ri, lambda - ι, versus radiation disk thickness - mm.

ι \ ρ	3.000	4.000	5.000
0.00020	0.547	0.997	1.401
0.00030	0.162	0.296	0.415
0.00040	0.068	0.125	0.175
0.00050	0.035	0.064	0.090

ρ = r0/ri, lambda - ι, versus Heat Leak Parameter, Qs/QL

ι \ ρ	3.000	4.000	5.000
0.00020	0.0615	0.0885	0.1093
0.00030	0.0273	0.0394	0.0486
0.00040	0.0154	0.0222	0.0274
0.00050	0.0099	0.0142	0.0175

ρ = r0/ri, lambda - ι, versus Rotor/Stator Stack Spacing mm

ι \ ρ	3.000	4.000	5.000
0.00020	1.641	2.992	4.203
0.00030	0.487	0.887	1.246
0.00040	0.205	0.374	0.526
0.00050	0.105	0.192	0.270

ρ = r0/ri, lambda - ι, versus number of rotor disks

ι \ ρ	3.000	4.000	5.000
0.00020	352	232	183
0.00030	791	521	412
0.00040	1405	925	732
0.00050	2195	1445	1143

ρ = r0/ri, lambda - ι, versus number of Stator disks

ι \ ρ	3.000	4.000	5.000
0.00020	353	233	184
0.00030	792	522	413
0.00040	1406	926	733
0.00050	2196	1446	1144

DISTRIBUTION LIST

AUL/LSE **Bldg 1405 - 600 Chennault Circle** **Maxwell AFB, AL 36112-6424**	**1 cy**
DTIC/OCP **8725 John J. Kingman Rd, Suite 0944** **Ft Belvoir, VA 22060-6218**	**2 cys**
AFSAA/SAI **1580 Air Force Pentagon** **Washington, DC 20330-1580**	**1 cy**
PL/SUL **Kirtland AFB, NM 87117-5776**	**2 cys**
PL/HO **Kirtland AFB, NM 87117-5776**	**1 cy**
Official Record Copy **PL/VTV/Marko Stoyanof** **Kirtland AFB, NM 87117-5776**	**2 cys**
PL/VT **Dr Hogge** **Kirtland AFB, NM 87117-5776**	**1 cy**

DEPARTMENT OF THE AIR FORCE
PHILLIPS LABORATORY (AFMC)

28 Jul 97

MEMORANDUM FOR DTIC/OCP
8725 John J. Kingman Rd, Suite 0944
Ft Belvoir, VA 22060-6218

FROM: Phillips Laboratory/CA
3550 Aberdeen Ave SE
Kirtland AFB, NM 87117-5776

SUBJECT: Public Releasable Abstracts

1. The following technical report **abstracts** have been cleared by Public Affairs for unlimited distribution:

PL-TR-96-1020	ADB208308	PL 97-0318 (clearance number)
PL-TR-95-1093	ADB206370	PL 97-0317
PL-TR-96-1182	ADB222940	PL 97-0394 and DTL-P-97-142
PL-TR-97-1014	ADB222178	PL 97-0300

2. Any questions should be referred to Jan Mosher at DSN 246-1328.

Jan Mosher
PL/CA

cc:
PL/TL/DTIC (M Putnam)